Available online at www.sciencedirect.com
SCIENCE DIRECT®
Precambrian Research 133 (2004) 75–103
Precambrian Research
www.elsevier.com/locate/precamres

Subaerial exposure surfaces in a Palaeoproterozoic ^{13}C-rich dolostone sequence from the Pechenga Greenstone Belt: palaeoenvironmental and isotopic implications for the 2330–2060 Ma global isotope excursion of $^{13}C/^{12}C$

V.A. Melezhik [a,*], A.E. Fallick [b], S.M. Grillo [c]

[a] *Geological Survey of Norway, Leiv Eirikssons vei 39, N-7491 Trondheim, Norway*
[b] *Scottish Universities Environmental Research Centre, East Kilbride, Glasgow G75 0QF, Scotland, UK*
[c] *Dipartimento di Geoingegneria e Tecnologie Ambientali, Facoltà di Ingegneria, Piazza D'Armi, 09123 Cagliari, Italy*

Received 9 September 2003; accepted 30 March 2004

Abstract

This article reports the discovery of numerous subaerial exposure surfaces which occur in the ca. 2200 Ma Kuetsjärvi Sedimentary Formation (KSF) from the Pechenga Greenstone Belt, NE Fennoscandian Shield, Russia. The formation was accumulated within an intraplate rift and is composed of fluviatile-deltaic siliciclastic deposits and lacustrine dolostones. The dolostones are enriched in ^{13}C ($\delta^{13}C = +6.6$ to $+7.6$‰ V-PDB, $\delta^{18}O = 16.7$ to 21.5‰ V-SMOW), which is, in general, assigned to a global perturbation of the carbon cycle. The lacustrine dolostone unit contains desiccated and in situ brecciated carbonate beds, subaerial erosion and dissolution surfaces, epikarst, surficial silicification (silcretes) and hot-water spring travertines. The dissolution surfaces—marked by formation of a few centimetre thick, 'vuggy', non-laminated, dolomicrite capped by silicified nodular zone—resemble modern calcretes which formed by capillary rise of surface waters (per-ascensum calcrete) following saturation of the regolith zone under arid or semi-arid conditions. Abundant red, iron-stained, superficial dolocrete implies the existence of an O_2-rich atmosphere. Rezolith, 'black pebbles', alveolar septal structures, '*Microcodium*' and other fabrics associated with plant roots and input of terrestrial organic matter, which are typical for post-Cretaceous pedogenic calcretes, have not been identified. Alfa fabrics can be applied to describe dolocretes though rhombic calcite crystals are lacking. Neither ^{13}C-depletion nor ^{13}C-enrichment has been documented in the dolocrete, which suggests no contribution of CO_2 derived from soil or from any other C_{org}-rich sources enriched in ^{12}C, and apparent lack of biological uptake of ^{12}C during formation of the dolocrete. Both petrographic and carbon isotope data do not support earlier assertions that Palaeoproterozoic subaerial surface was colonised by microbial mats. A few samples have high $\delta^{18}O$ values (up to 30‰) despite diagenetic and metamorphic resetting of the oxygen isotope system, suggesting evaporation during formation of the superficial dolocrete. Such documented episodes of subaerial exposure, formation of hot-water travertines, superficial dolocrete and silcrete suggest that there must have been frequent decoupling between the Kuetsjärvi depositional system and the bordering sea. This imposes an additional restriction on the use of the isotopic composition of the KSF dolostones for reconstruction of the $\delta^{13}C_{carb}$ global secular curve.

Keywords: Palaeoproterozoic; Lacustrine; Dolocrte; Silcrete; Dolostone; Carbon and oxygen isotopes; Subaerial exposure surface

* Corresponding author. Tel.: +47-73-90-40-11; fax: +47-73-92-16-20.
E-mail address: victor.melezhik@ngu.no (V.A. Melezhik).

0301-9268/$ – see front matter © 2004 Elsevier B.V. All rights reserved.
doi:10.1016/j.precamres.2004.03.011

1. Introduction

Several subaerial exposure features have been discovered in the Palaeoproterozoic Kuetsjärvi Sedimentary Formation (KSF) of the Pechenga Greenstone Belt, north-west Russia (Fig. 1a). This formation is temporally associated with the Palaeoproterozoic positive isotopic excursion of carbonate carbon (Karhu and Melezhik, 1992; Melezhik and Fallick, 1996) which occurs world-wide at ca. 2200 Ma (Schidlowski et al., 1976; Baker and Fallick, 1989a,b; Yudovich et al., 1991; Karhu, 1993; Melezhik et al., 1997, 1999; Buick

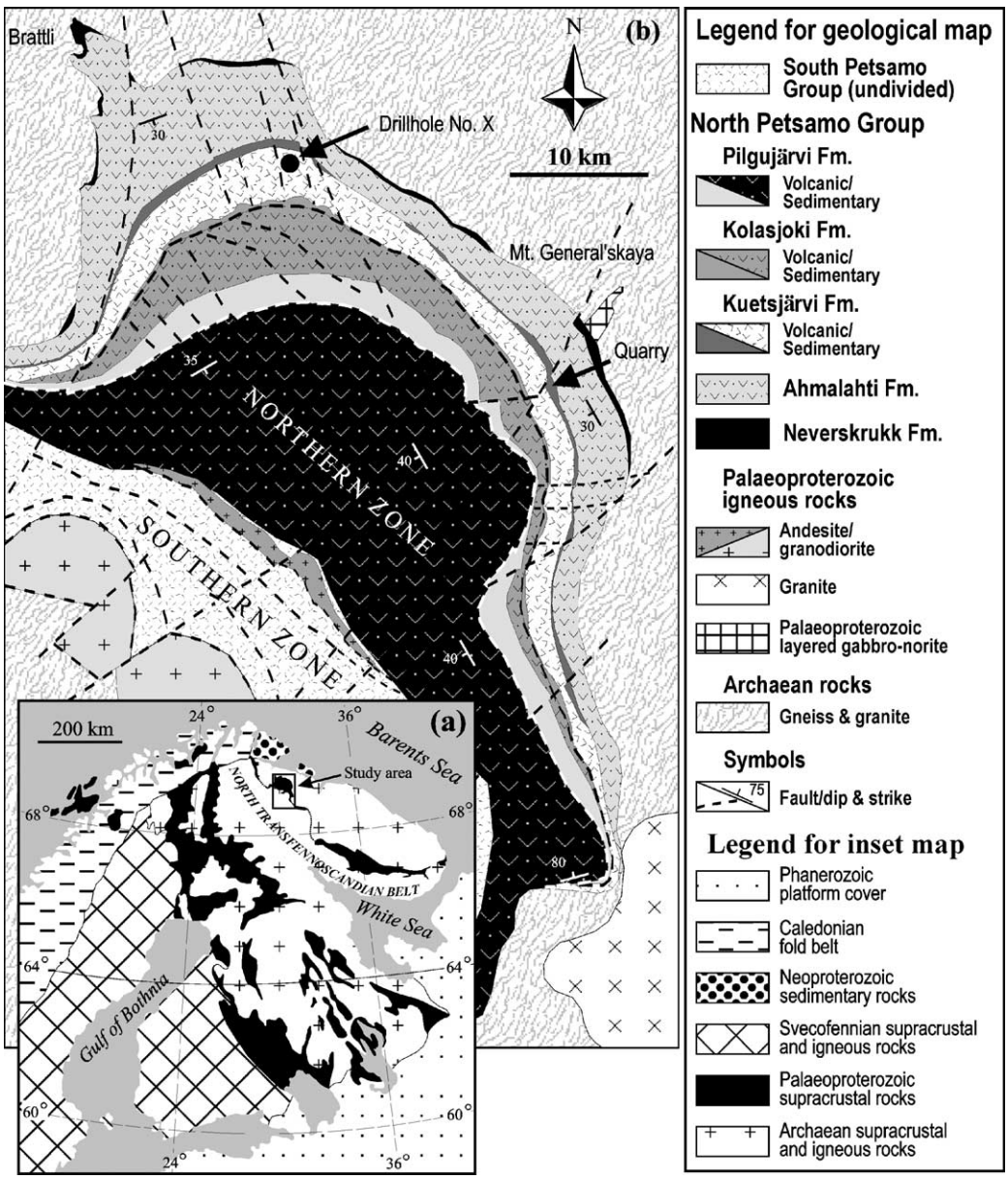

Fig. 1. (a) Geographic and geological location map of the study area (inset map), and (b) simplified geological map of the Pechenga Greenstone Belt.

et al., 1998; Bekker et al., 2001, 2003). In a series of publications (e.g., Melezhik et al., 1999, 2000) we have suggested that the extremely high $\delta^{13}C$ values (well above +5‰) measured from Palaeoproterozoic dolostones were perhaps related to restricted environments. However, in general, there are obvious difficulties in differentiating between open marine and restricted environments in the Precambrian due to the dominance of tectonically fragmented and metamorphosed sequences, and the absence of fossils. Features of subaerial exposure are important because they may suggest a degree of the basinal restriction and decoupling from the neighbouring sea.

Palaeosols, calcretes, palaeokarsts, records of vadose-zone cementation, cement stratigraphic discontinuities, fluid inclusions and the C and O isotopic records are important for identifying ancient events of subaerial exposure (Goldstein et al., 1991; Alonso-Zarza, 2003). In ancient complexes, the cementation history and the composition of fluid inclusions can be severely overprinted by various post-depositional processes and therefore have limited utility. There are two major diagenetic carbonate facies associated with subaerial exposure, namely karst and calcrete facies (Esteban and Klappa, 1983), which have potential to be preserved in ancient rocks (Chown and Caty, 1983; Bertrand-Sarfati and Moussine-Pouchkine, 1983; Horodyski and Knauth, 1994; Knauth et al., 2003). In the karst facies there is a net loss of calcium carbonate, whereas in the calcrete facies there is a zero balance or a net gain from elsewhere (Esteban and Klappa, 1983). Although processes operating in both karst and calcrete diagenetic environments are not mutually exclusive, calcrete is attributed to a semiarid climatic zone (Goudie, 1973), whereas karst facies develops in all climates with water (Esteban and Klappa, 1983).

Subaerial exposure surfaces developed on carbonate rocks are well documented in the geological record from Silurian–Devonian times onward (Woodrow et al., 1973; Esteban and Klappa, 1983). Precambrian (Bertrand-Sarfati and Moussine-Pouchkine, 1983) and Early Palaeozoic (Johnson and Swett, 1974) occurrences are sparse and present more problems for interpretation (Sochava et al., 1975). It has also been suggested that before the Silurian, karst and calcrete facies might have different features, because of the absence of the influence of higher plants (Esteban and Klappa, 1983). One major difference could have been the lack of ^{12}C-rich biogenic CO_2 obtained from terrestrial vegetation.

Calcrete deposits in ancient sedimentary successions are of importance because they indicate subaerial exposure without detrital sedimentation for a significant period of geological time (Demicco and Hardie, 1994; Alonso-Zarza, 2003). Thus, the presence of calcrete implies the existence of a subaerial 'omission surface' that results from the complete cessation of sedimentation in what was once an active site of deposition.

The major objectives of this paper are to: (i) describe various sedimentological features suggesting subaerial exposures in ^{13}C-rich KSF dolostones, (ii) discuss the palaeoenvironmental significance of subaerial exposures, and (iii) contribute to a better understanding of depositional environments of carbonates during the course of the Palaeoproterozoic positive isotopic excursion of $^{13}C/^{12}C$ in sedimentary carbonates.

2. General stratigraphy and age

The KSF belongs to the Pechenga Greenstone Belt which is part of a larger, discontinuous belt stretching over a distance of 1000 km in the north-eastern part of the Fennoscandian Shield (Fig. 1). The KSF was deposited in an intracratonic rift system (Melezhik and Sturt, 1994). The formation ranges from 20 to 120 m in thickness and consists of lower Quartzite and upper Dolostone Members. The Quartzite Member lies on weathered, subaerially erupted amygdaloidal basaltic andesites of the Ahmalahti Volcanic Formation (Figs. 1 and 2). The lower part of the Quartzite Member starts with a large-scale coarsening-upwards deltaic sequence consisting of grey, graded sandstone-siltstone beds with rare thin beds of dolostones (Melezhik and Fallick, in press). This sequence is followed by variegated, hematite-rich, lacustrine siltstones and mudstones with thin horizontal, varved-like lamination. The upper part of the KSF is composed of a ca. 80 m thick unit of dolostones comprising the Dolostone Member (Fig. 2). These are interbedded allochemical, micritic dolostones and flat-laminated, dolomitic stromatolites. Stromatolitic lamination is disrupted by desiccation cracks and microbrecciation. A larger scale

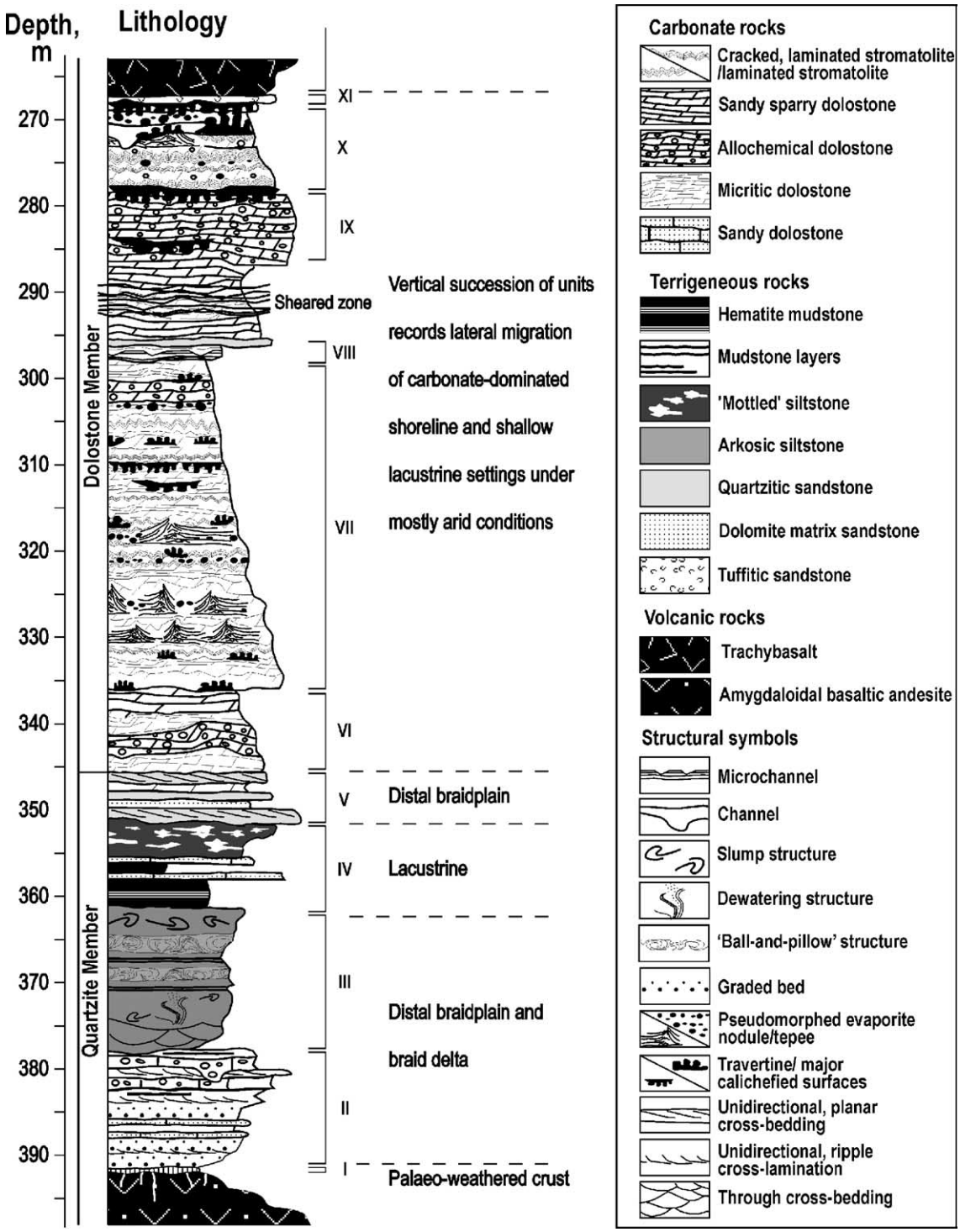

Fig. 2. Simplified lithological section of the KSF as it appears in DH X (Melezhik and Fallick, 2001, modified).

brecciation is related to the development of tepee structures (Melezhik and Fallick, in press). In places, the micritic and stromatolitic dolostones contain micronodules of apparent evaporites pseudomorphed by chert and dolomite. Hot-water spring travertine crusts are abundant throughout the carbonate unit (Melezhik and Fallick, 2001). The Dolostone Member is overlain by 2000 m thick, subaerially deposited volcanic rocks of the Kuetsjärvi Volcanic Formation.

The lower age limit of the Pechenga Belt rocks is younger than the emplacement of the layered gabbro-norite (2505 ± 1.6 Ma, U–Pb on baddelyite, Amelin et al., 1995) incorporated as clasts into basal Pechenga conglomerates. The upper age limit, based on Sm–Nd (minerals) and U–Pb (zircon) methods, is older than 1990 Ma (Hanski et al., 1990). Available radiometric ages constrain the Palaeoproterozoic $\delta^{13}C_{carb}$ positive excursion occurring on the Fennoscandian Shield to between 2330 and 2060 Ma (Karhu, 1993). The KSF underwent diagenesis, metamorphism and concomitant deformation during the ca. 1850 Ma Svecofennian orogeny.

3. Sedimentary features of subaerial exposures

Determining subaerial exposures and depositional history of the KSF is based on characterisation of various features indicating phases of emergence. This includes desiccation, erosional and dissolution surfaces, and palaeosol horizons.

3.1. Desiccated and in situ brecciated dolostone and mudstone beds

3.1.1. Observations

Beds of micritic and algal, stromatolitic dolostone occurring in the Quartzite Member (Fig. 2) show discontinuous development, limited thicknesses of 1–15 cm and intensive in situ brecciation (Fig. 3a). In plan, the dolostone beds appear as completely disconnected polygons. Cross-sections show ‘V’ shapes to wide, parallel-walled fissures. Some dolostone beds have been split up, by planar cracks parallel to the bedding, in to several sheets resulting in complex, brecciated cross-sections (Fig. 3a). Both the vertical and sheet crack infill is composed of clayey sandstone as well as dolostone debris spalled off crack walls. Often, the clayey sandstone from the layer above the desiccated dolostone can be traced directly down into the crack fill.

The brecciated dolostone beds are commonly associated with thin mudstone layers showing irregularly developed polygonally-cracked surfaces (Fig. 3b). Crack infill is composed of the clayey sandstone.

Numerous beds of algal, stromatolitic dolostone occurring in the Dolostone Member (Fig. 2) show intensive cracking (Fig. 3c). Cross-sections show tight, subparallel-walled fissures. Sheet cracks are defined by a millimetre-scale, bedding-parallel laminoid voids (Fig. 3c) which do not exhibit any traces of enlargement by solution. Both vertical and sheet cracks are filled with microcrystalline quartz and dolospar containing minor angular clasts of internal sediment.

3.1.2. Interpretation

The cracked and brecciated dolomicritic, stromatolitic and mudstone beds show patterns which are diagnostic of dewatering and desiccation during subaerial exposure and soil processes (Brewer, 1964; Freytet and Plazait, 1982). Mudcracks are considered one of the most useful sedimentary features for identifying subaerial exposure in ancient carbonate flat environments (Klappa, 1980; Shinn, 1983,1986; James, 1984; Demicco and Hardie, 1994). The fabric in which clasts can no longer be fitted together (Fig. 3a), indicates extensive brecciation and water infiltration (Mazzullo and Birdwell, 1989; Wright, 1990).

3.2. Subaerial erosion surfaces

3.2.1. Observations

Several channels have been documented in the Quartzite Member (Fig. 2). These channels incise into sandstones down to 50 cm and are infilled with either poorly sorted dolarenite (Fig. 3d) or matrix-supported flat-pebble conglomerates, where tabular fragments of micritic dolostone are emplaced in silty matrix.

Erosion surfaces in the Dolostone Member are abundant. The scale of erosion varies from micro to macro. The small-scale erosion surfaces have a limited lateral extent of a few tens of centimetres. Cross-sections show irregular relief (in order of a few centimetres) with clearly truncated primary lamination and small debris of eroded rocks in topographic lows. The eroded surfaces are either coated with laminated

travertine (Fig. 3e) or filled with unsorted dolarenites. In plan, when the erosion surfaces are covered with the travertine, they appear as travertine-supported dolomite microbreccia with complex internal structure. Larger-scale erosion features are represented by uneven surfaces with relief in order of several tens of centimetres. Such erosion surfaces are commonly covered by travertine crusts and filled with dolomite-cemented sandstones and dolarenites (Fig. 3f).

3.2.2. Interpretation

The channels occurring in the Quartzite Member (Fig. 3d) have been interpreted as crevasse channels developed in the deltaic clastic sequence (Melezhik and Fallick, in press). The dolarenite infill suggests that the previously deposited carbonate material was exposed to air with subsequent erosion and transportation by the alluvial system in subaerial environments.

The cause of erosion surfaces in the Dolostone Member is considered to be uplifting and blocking during rift propagation. This might have resulted in the formation of tilted blocks (Fig. 3f), small horst and grabens with subsequent erosion on newly formed relief. However, the eroded surfaces created by these processes cannot alone be used as proof of subaerial exposure because faulting and blocking could also occur in a subaqueous environment. In this case, the hot-water travertine crust covering different-scale erosion surfaces is used as an unequivocal criterion of subaerial exposure because modern and ancient travertines have been only found in subaerial environments like coastal marshes, lake shores, springs, rivers, and waterfalls (e.g., Demicco and Hardie, 1994). In the studied case, the travertine, coating erosion surfaces, was categorised as autochtonous travertine formed from hot water springs (Melezhik and Fallick, 2001).

Fig. 3. Sedimentological characteristics of various subaerial exposure surfaces in the KSF as documented in natural exposures and drillcore material. (a) Cross-section view of natural outcrop showing micritic dolostone beds with intensive desiccation and in situ brecciation. Desiccation features are represented by both sheetcracks (arrowed in red) developing parallel to the bedding and by sub-vertical cracks (arrowed in black). Both crack systems are infilled with pale brown clayey sandstone. Exposure in the central part of the Pechenga Belt, 7 km west of DH X (Fig. 1); the upper part of the Quartzite Member (Fig. 2). Pencil—15 cm. (b) Polygonally-cracked surface of mudstone layer interbedded with the desiccated dolostones shown in (a). Exposure in the central part of the Pechenga Belt, 7 km west of DH X (Fig. 1); the upper part of the Quartzite Member (Fig. 2). Hammer head—15 cm. (c) Photomicrograph in transmitted non-polarised light showing cross-section view of intensively cracked stromatolitic dolostone. Desiccation features are represented by both mudcracks (arrowed in black) and sheetcracks (arrowed in red). The crack infill is mainly composed of dolosparite and microcrystalline quartz. Sample from DH X, depth 273.55 m; the upper part of the Dolostone Member. (d) Cross-section view through subaerial erosion channel (arrowed in red) cutting through pale purple arkosic sandstone and dark purple, hematite-rich siltstone. Channel is infilled with poorly sorted dolarenite showing irregularly developed dolomitisation (D). Exposure in the central part of the Pechenga Belt, 8.2 km west of DH X (Fig. 1); the upper part of the Quartzite Member. Pencil—15 cm. (e) Photomicrograph in transmitted non-polarised light showing cross-section through eroded surface (arrowed in red) developed on laminated dolomicrite (LDM). The eroded surface and dolomicrite clasts (DC) are veneered by travertine crust composed of fibrous dolomite (FTD). Sample from DH X, depth 309 m (Fig. 2); the middle part of the Dolostone Member. (f) Cross-section view through large erosion surface developed in dolostone. The erosion surface extends from left side downwards to lower right corner (arrowed in red) and is covered with pale grey, travertine crusts (TD_1, above red arrows) followed by thicker crust of beige and pale pink, finely laminated travertine (TD_1, below yellow arrows). The travertine-covered, uneven palaeorelief is filled with dolomite-cemented sandstone (DCS), which is in turn followed by sub-horizontally lying dolarenite beds (DA) with 'wavy' upper surface capped by 1–12 cm thick travertine crust (TD_2, between blue arrows). Photograph was taken from the quarry, 30 km south-east of DH X (Fig. 1); the middle part of the Dolostone Member (Fig. 2). Pencil—15 cm. (g) Polished slab illustrating vertical section of hot-water laminated travertine crust (LTD) with dissolution pipes (DP) and trough-like dissolution cavity (DT) of surface origin. The trough cavity cuts trough the travertine crust down in to underlying micritic dolostone (MD). Dissolved surface of the travertine and trough-like cavity is veneered by silica sinter (SS). Sample was collected from the quarry, 30 km south-east of DH X (Fig. 1); the middle part of the Dolostone Member (Fig. 2). (h) Polished slab illustrating vertical section of hot-water laminated travertine crust (LTD) with small dissolution pipe (DP) and several dissolution trough-like cavities (DT) of surface origin. The dissolved surface of the travertine and trough-like cavities are veneered by silica sinter (SS). The underlying dolostone shows numerous sub-horizontal, bedding-parallel, laminoid voids filled with fibrous travertine dolomite (FTD). Sample was collected from the quarry, 30 km south-east of DH X (Fig. 1); the middle part of the Dolostone Member (Fig. 2). (i) Polished slab illustrating vertical section trough sandy micritic dolostone (SMD) with dissolution cavity of surface origin. Surface of the cavity is veneered with red dolocrete (DC, arrowed in black) and grey silcrete (S, arrowed in white). The cavity is filled with sandy, allochemical dolostone (SAD) which is overlain by pale pink, fine-pebble, dolomite conglomerate (DCNG). Sample was collected from the quarry, 30 km south-east of DH X (Fig. 1); the middle part of the Dolostone Member (Fig. 2). (j) Polished slab illustrating vertical section through epikarstic cavity which is filled with quartz sandstone. Floor and roof of the cavity are coated

Fig. 3. (*Continued*)
with pale grey and white, laminated, travertine crusts with small 'stalagmites' and 'stalactites'. Red arrows indicate growth direction of the travertine dolomite. Sample was collected from the quarry, 30 km south-east of DH X (Fig. 1); the uppermost part of the Dolostone Member (Fig. 2). (k) Cross-section view through epikarstic cavity veneered by hot-water travertine dolomite (TD). Floor of the cavities is made of small-scale travertine mounds ('stalagmites'), whereas the roof is coated by travertine crusts with undulating surface. Remaining space is filled with red, hematite-rich, laminated, muddy sandstone and mudstone (RS, redeposited *terra-rossa*?). Red arrows indicate growth direction of the travertine dolomite. Sample was collected from the quarry, 30 km south-east of DH X (Fig. 1); the middle part of the Dolostone Member. (l) Polished slab showing cross-section through dolomite-cemented sandstone (DCS) veneered by colour-banded, laminated, dolomicritic, travertine crust (LTDM), which is followed by red, iron-stained, non-laminated dolomicrite (IDM) with dissolution vugs (DV) capped by silicified nodular zone (SNZ). The silicified nodular zone (arrowed in blue) is overlain by sandy micritic dolostone (SMD). Sample was collected from the quarry, 30 km south-east of DH X (Fig. 1); the upper part of the Dolostone Member (Fig. 2). (m) Photomicrograph in transmitted non-polarised light showing composite cross-section through the following zones: zone (i)—laminated (LTDM) and non-laminated (NLTDM) travertine dolomicrite filling surficial erosion cavity in dolomite-cemented sandstone (DCS); zone (ii)—fractured, iron-stained, non-laminated dolomicrite (IDM); zone (iii)—dissolution breccia; zone (iv)—silicified nodular zone (SNZ). The silicified nodular zone (SNZ) is ovelain by sandy dolomicrite (SDM) showing no silicifcation. The travertine crust (NLTDM + LTDM) contains quartz-pseudomorphed, zoned, rhomboidal crystals of probable gypsum (G) and shows uneven, dissolved upper surface (arrowed in red). Large, white arrow indicates direction growth of the travertine dolomite. The iron-stained, non-laminated dolomicrite (IDM) of zone (ii) has formed on uneven, dissolved surface of the travertine crust (arrowed in red). Fractures (IF) developed in the iron-stained dolomicrite (IDM) are enlarged by solution and filled with microdolospar and microcrystalline silica. The fractures do not extend in to the travertine crust (zone i). The smooth, irregular, dissolved, upper surface of zone (ii) is unevenly lined with earlier isopachous dolomite cement (ID). Fragments of the iron-stained, non-laminated dolomicrite (IDM) in solution breccia (zone iii) show more intensive iron-staining compared with similar dolomicrite (IDM) of zone (ii). Fragments are cemented by partially silicified dolomicrite (SDM), whereas remaining space is filled with dolospar (DS). All earlier fabrics are crosscut by later, metamorphic veinlet filled with dolomite and quartz (MV). Sample was collected from the quarry, 30 km south-east of DH X (Fig. 1); the lower part of the Dolostone Member (Fig. 2). (n) Photomicrograph in transmitted non-polarised light showing cross-section through zone (iii). 'Vuggy', iron-stained, non-laminated dolomicrite (IDM) appears as solution breccia where all fragments are still intact. Solution cavities have smooth walls, which are unevenly lined by earlier isopachous dolomite cement (ID). Dolomicrite clast (DMC) is coated with earlier microdolospar (MDS) and then, by multiple generation of pendant cement (PC). Below the pendant cement, there are several partially dissolved, quartz grains (Q) suspended in dolomicrite (DM). Larger vug is filled with late equant dolospar (DS). Upper part of the breccia zone exhibits partially silicified dolomicritic cement (SDM) and contains nodular dolomicrite (NDM) and solitary silica micronodules (SN). Some silica micronodules are coated by microdolospar (MDS). Irregular fractures (IF) developed in the red, non-laminated dolomicrite (IDM) are enlarged by solution and filled with microdolospar and microcrystalline silica. All earlier fabrics are crosscut by metamorphic quartz-dolomite veinlet (MV). Sample was collected from the quarry, 30 km south-east of DH X (Fig. 1); the lower part of the Dolostone Member (Fig. 2). (o) Photomicrograph in transmitted non-polarised light showing cross-section through the silicified nodular zone (iv) developed on dissolved surface of the fractured (IF) iron-stained, non-laminated dolomicrite (IDM). Zone (iv) contains nodular (glaebular) dolomicrite (NDM) suspended in intensively silicified dolomicritic and microdolosparitic cement. Silica mostly replaces earlier dolomicritic cement, some dolomicrite nodules (NDM arrowed in red) and occurs as micronodules (SN) and silica crust (S). Some grains (MCG), however, show multiple coating by dolomicrite and silica, thus indicating a complex diagenetic history. Sample was collected from the quarry, 30 km south-east of DH X (Fig. 1); the lower part of the Dolostone Member (Fig. 2). (p) Cross-section view through dolarenite (DA) containing white, laminate travertine dolomite crusts (LTD). Red, iron-stained, non-laminated dolomicrite (IDM) sandwiched between colour-banded, laminated, travertine (CBLT) occurs on top of the lower white travertine crust. The dolarenite contains platy clast of the colour-banded, laminated, travertine (TC). Vertical wall in the quarry, 30 km south-east of DH X (Fig. 1); the middle part of the Dolostone Member (Fig. 2). (q) Section cutting travertine mound's head parallel to the bedding surface exhibits a series of concentric bands of fibrous dolomite (TD). Outer dolomite rim is veneered by silica sinter (S) which exhibits a replacive relationship to the underlying travertine layer. The silica-veneered travertine mound is emplaced in red sandstone (RS). Specimen was collected from the dolomite quarry, 30 km south-east of DH X (Fig. 1); the middle part of the Dolostone Member (Fig. 2). (r) Photomicrograph in transmitted non-polarised light showing cross-section through fibrous travertine dolomite travertine (TD) veneered by silica sinters (S) and overlain by sandstone (S in red). The lower sinter (red arrows) exhibits a replacive relationship to the underlying travertine layer. The upper sinters shows desiccation (white arrows), whereas the middle sinter was fragmented and emplaced in black, hematite-rich muddy material (MS), which also separates the lower and upper sinters. Sample was collected from the quarry, 30 km south-east of DH X (Fig. 1); the middle part of the Dolostone Member (Fig. 2). (s) Polished slab illustrating travertine crust (TD) deposited on uneven surface (arrowed in red) of pink, micritic dolostone (PMD) which shows abundant bedding-parallel, laminoid voids extending from the bedding surface downwards. Voids are walled and filled with travertine dolomite (D) resulting in macro-clotted fabrics. Sample was collected from the quarry, 30 km south-east of DH X (Fig. 1); the middle part of the Dolostone Member (Fig. 2). Height of specimen—17 cm. (t) A stack of travertine crusts (arrowed) developed in dolarenite (DA). The photograph was taken from the dolostone quarry, 30 km south-east of DH X (Fig. 1); the middle part of the Dolostone Member (Fig. 2). Scale bar: 10 cm.

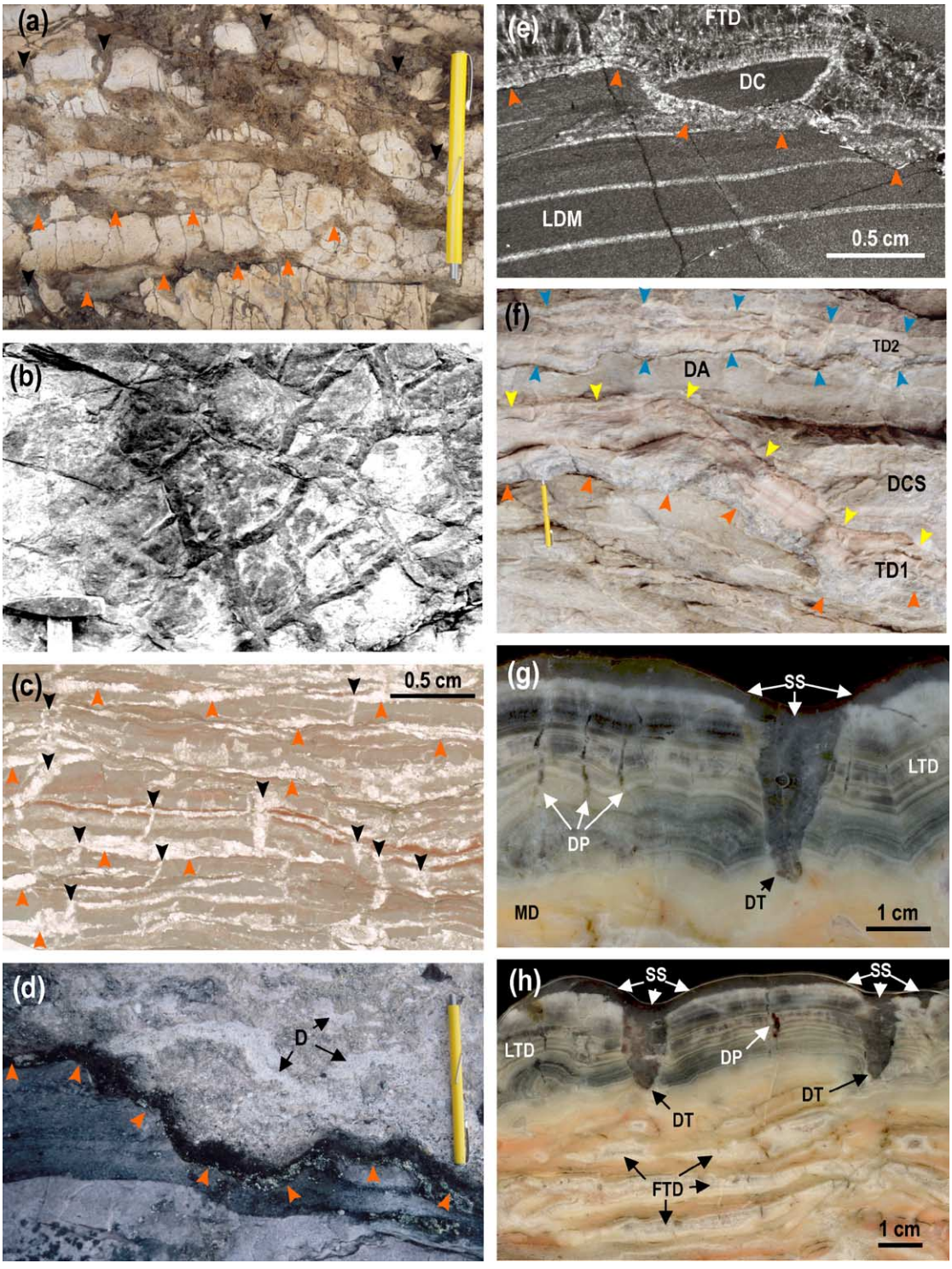

Fig. 3 (*Continued*)

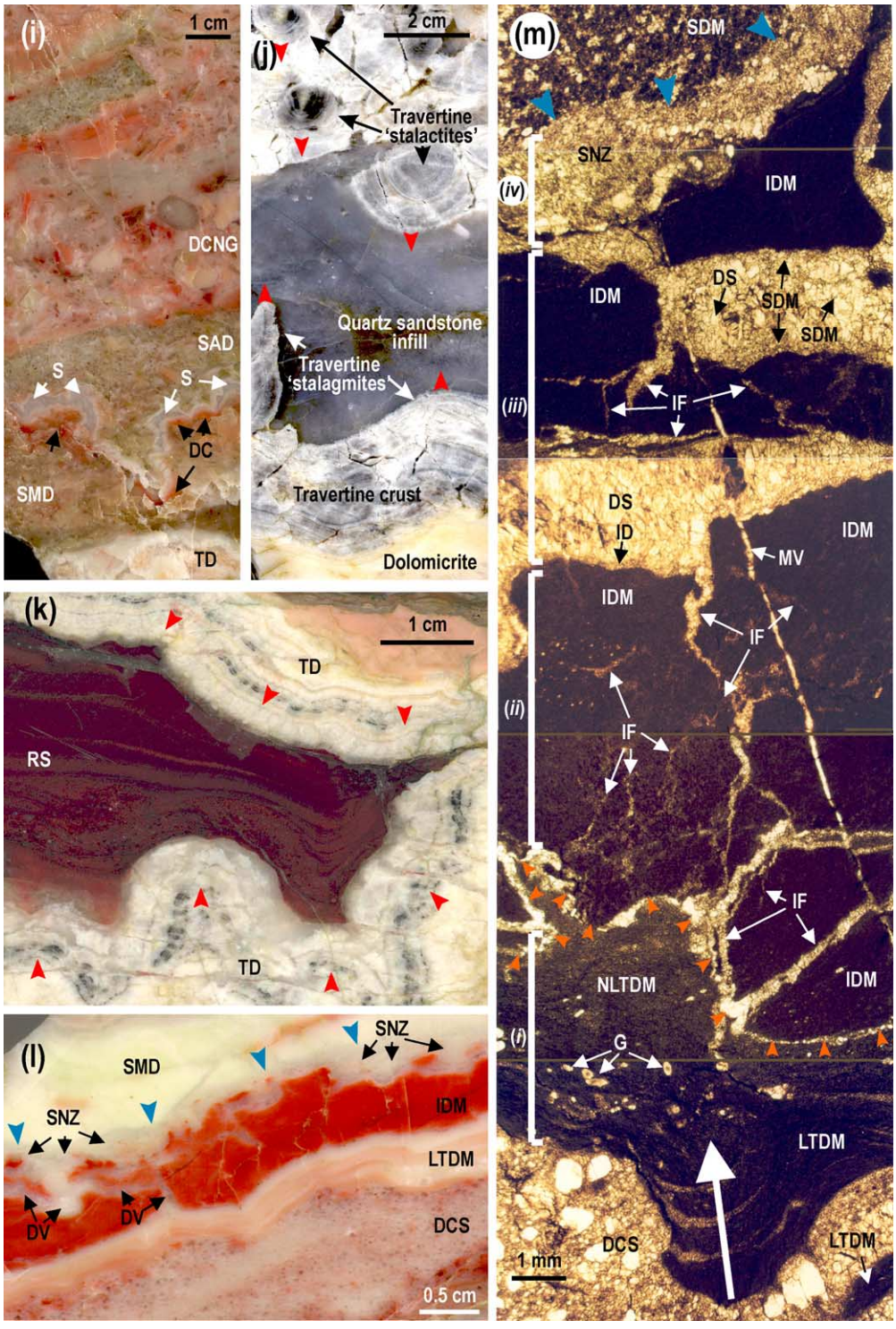

Fig. 3 (*Continued*)

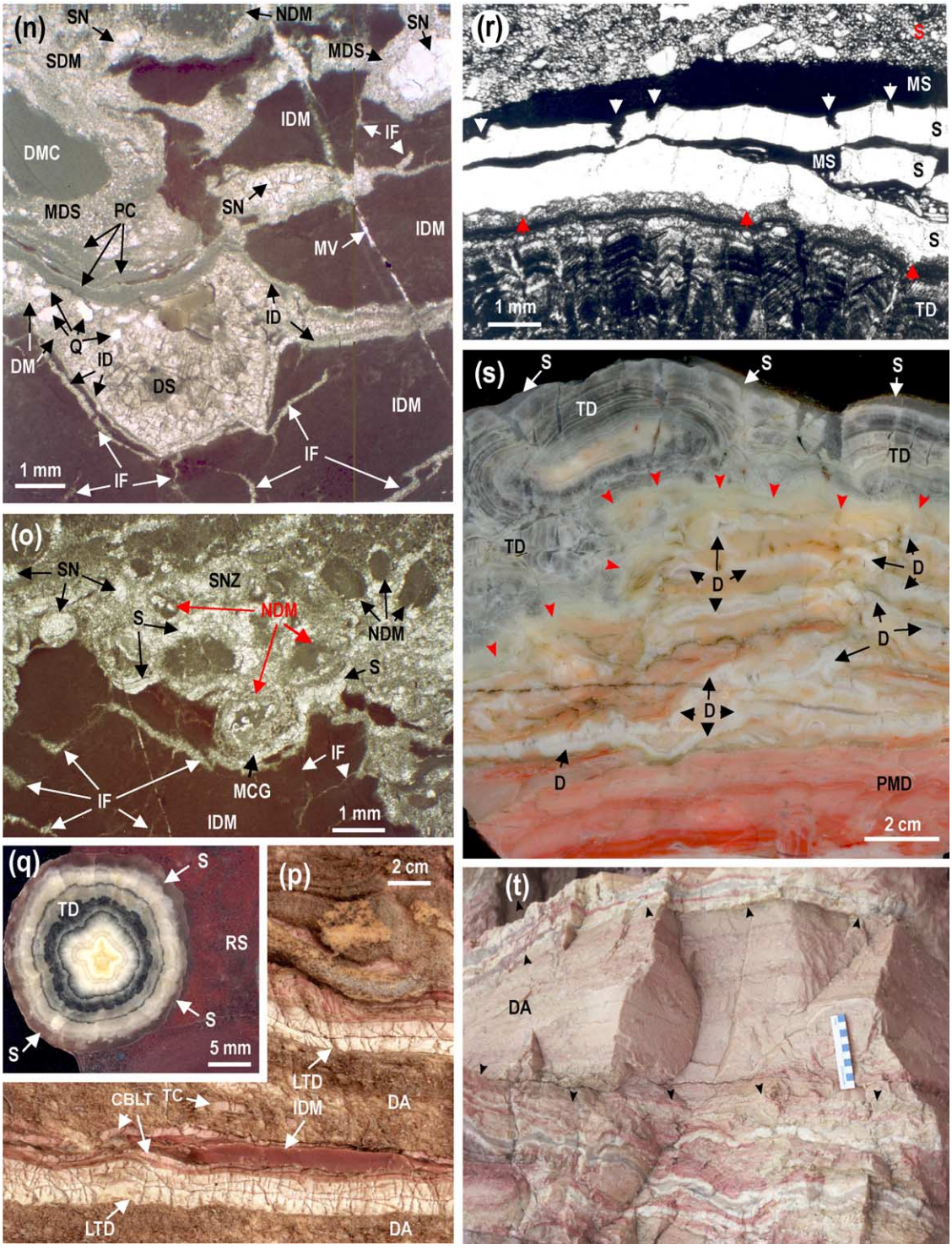

Fig. 3 (*Continued*)

3.3. Subaerial dissolution surfaces and epikarst

3.3.1. Observations

Bedding planes affected by formation of vugs and microcavities have been observed developing on different carbonate substrates of the Dolostone Member. The travertine crusts have been most affected by formation of vugs and microcavities. In plan, microcavities vary from linear to irregularly developed polygonal network systems of a limited areal extent in the order of a few square meters. Cross-sections show two different morphologies. The dominant are a through-like cavities that extend from the bedding surface downwards over a depth of 1–5 cm (Fig. 3g and h). The second morphology is tiny, millimetre-scale, vertical tubes extending from the bedding surface downwards over a depth of 1–3 cm (Fig. 3g and h). Both the through-like cavities the vertical tubes exhibit enlargement by solution and are veneered by finely crystalline silica sinters (Melezhik and Fallick, 2001).

Commonly, dolostone surfaces beneath the travertine crusts show abundant voids. The latter occur just below the bedding surface in the form of millimetre-scale, bedding-parallel, lensoidal or laminoid voids. They often occur roughly aligned in layers and are linked by short transverse connections (Fig. 3h). The voids exhibit enlargement by solution and are walled and filled with inward-growing travertine dolomite.

The microcavities have also been observed in sandy micritic dolostones where they have 'V'-shape in cross section, with depth of 2–5 cm (Fig. 3i). The microcavities truncate bedding and affect crystals and grains. Surfaces of such cavities are commonly veneered by thin, irregularly developed, red dolomicrite and silcrete (Fig. 3i). The silcrete has a corrosive relationship with the underlying dolomicrite; however, it does not affect overlying dolarenites and dolorudites that fill the dissolution cavities (Fig. 3i).

In the upper part of the Dolostone Member, the size of voids and cavities reaches a scale of several tens of centimetres. These larger scale cavities are developed irregularly and coated with the travertine (Fig. 3j). In most cases, the floor and the roof of cavities are coated with beige and yellowish, finely laminated travertine crusts with rare 1–5 cm high 'stalagmites' and 'stalactites'. The remaining space is filled with either a quartz sandstone (Fig. 3j) or a chlorite-rich, structureless, dolarenite mass. The latter may contain large fragments of yellowish, finely laminated travertine mounds as well as 1–5 mm-thick crusts of fibrous travertine which shows synsedimentary fragmentation. In other cases travertine covering the floor of cavities is represented by small-scale mounds ('stalagmites'), whereas the roof is coated by travertine crusts with undulating surface. The remaining space is filled with red and brown, hematite-rich, laminated, muddy sandstone and mudstone resembling redeposited *terra-rossa* (Fig. 3k).

3.3.2. Interpretation

The through-like cavities and vertical tubes developed on the subaerially formed hot-water travertine crusts show several features which are consistent with their superficial origin by solution: (i) extend from the surface downwards, (ii) enlargement by solution, and (iii) cementation by silica sinters. The corrosive relationship of the silica sinters with the underlying substrates, without such effect in respect of overlying sedimentary material, suggests that their formation took place prior to deposition of the overlying rocks. Thus, the silica-veneered cavities can be interpreted as a surface solution feature.

The bedding-parallel, lensoidal or laminoid voids, which occur beneath travertine crusts (Fig. 3h), served as conduits for thermal, travertine-depositing waters. The voids have apparently formed due to solution by unsaturated waters percolating through dolostone beds. Planar and horizontal shape of the voids may also indicate a desiccation origin as described by Brewer (1964) and Freytet and Plaziat (1982). Alternatively, they may be compared to the buckle cracks of the calcretes of Texas and New Mexico (Reeves, 1970). At any rate, they suggest subaerial exposure surfaces.

The larger cavities infilled with the travertine 'stalactites' and 'stalagmites' (Fig. 3j and k) exhibit several features which have been described for karst (Esteban and Klappa, 1983). However, the scale of the studied solution forms are much smaller than usually applied for karst, and therefore a term *superficial epikarst* (e.g., Klimchouk, 1997) appears to be more appropriate. The cavities existed before the growth of the travertine 'stalagmites' and 'stalactites'. They remain located in the subaerial environment during the travertine deposition and receive sediments carried by flowing waters (Fig. 3j and k).

3.4. Dolocrete

3.4.1. Observations

Numerous 0.5–5 cm-thick crusts consisting of laminated and non-laminated dolomicrite and partially silicified orbicular rocks (Fig. 3l) occur throughout the Dolomite Member. These crusts are developed on different carbonate substrates, though each individual crust has a limited areal extent in the order of a few square metres. The complete vertical profile of such crusts includes (i) 0.2–3 cm-thick colour-banded dolomicrite laminae; (ii) red to brown, non-laminated dolomicrite; (iii) 'vuggy', dolospar-cemented, dolomicrite and breccia; and (iv) zone of orbicular silicified rocks (Fig. 3m). Commonly, the vertical profile consists only zones (iii) and (iv).

The colour-banded, thinly laminated (millimetre-thick) dolomicrite (Figs. 3l and m) was deposited on sandy micritic dolostones and dolomite-cemented sandstones (Fig. 3m). The colour-banded dolomicrite is flat laminated (Fig. l and m, zone (i)) and passes upwards in to a beige, non-laminated dolomicrite. The dolomicrite laminites follow the irregularities and fill the depressions of the substrate (Fig. 3m), thus accreting upwards. Individual laminae display conformable contacts. Bands in the crust are due dominantly to differential staining and crystal size. Desiccation features, fenestrae and vugs are lacking. Both the colour-banded, laminated and the beige, non-laminated micrite contain irregular scattered clusters of zoned rhomboidal crystals resembling gypsum replaced by quartz (Fig. 3m).

The red dolomicrite of zone (ii) either conformably overlies the colour-banded dolomicrite laminae (Fig. 3l) or lies on its dissolved, irregular surface (Fig. 3m). The red dolomicrite does not show any lamination and is characterised by dense fabric and intensive red or brown staining (Fig. 3l and m) due to a dense impregnation by finely disseminated hematite particles. The red dolomicrite is affected by thin, irregularly developed fractures filled with microdolospar and microcrystalline silica (Fig. 3m, zone ii). The fractures widen upwards where they are connected and developed in to larger vugs, which give rise to the red 'vuggy' dolomicrite of zone (iii).

The 'vuggy' dolomicrite has either transitional contact with the underlying red dolomicrite (Fig. 3l) or is separated from it by an irregular surface (Fig. 3m, zone iii). The 'vuggy' dolomicrite is characterised by numerous irregular fenestrae, vugs and microcavities which are commonly connected by channels and form a complex network system resembling a miniature karst (Fig. 3m and n). In cross-sections such rocks appear as microbreccia where, after detachment from their substrate, fragments mainly stay intact (Fig. 3n). The clasts in the microbreccia are similar in composition to the dolomicrite of zone (ii), though are more intensely stained (Fig. 3m). Cavity walls have smooth surfaces, which suggests leaching and dissolution. Some vugs contain clasts of a non-stained dolomicrite and partially corroded quartz grains suspended in microdolosparitic matrix (Fig. 3n). The fenestrae, vugs, microcavities and fractures are cemented with multiple generations of cement. The earlier generation is represented by unevenly developed dolomicritic and isopachous dolomite cement lining cavities (Fig. 3n) as well as by clast-coating dolomictite and dolomicrospar (Fig. 3n). Pendant dolomicrite cement also shows multiple generations (Fig. 3o). The latest cement is the equant dolospar filling voids and finely crystalline silica replacing earlier dolomite (Fig. 3m and n).

The amount of the silica sharply increases in the upper 2–5 mm-thick zone (iv) which results in formation of the silicified crust (Fig. 3m, zone iv; Fig. 3o). The silicified zone contains coated dolomicrite grains, grey dolomicrite micronodules or glaebules suspended in dolomicrite and dolomicrospar cement. Thus, zone (iv) can be categorised as the nodular or orbicular crust (Fig. 3o). The silica replaces earlier dolomicrite cement and dolomicritic micronodules. Some micronodules show multiple replacement by silica (Fig. 3o). Silica also occurs in the form of micronodules and incrustations (Fig. 3o). The micronodules are composed of megaquartz coated by microcrystalline quartz. The silicified micronodules crust is sharply overlain by either a sandy dolostones or a dolomite-cemented sandstone showing no sign of 'nodularisation' and silicification (Fig. 3m).

3.4.2. Interpretation

The colour-banded, thinly laminated dolomicrite (Fig. 3l and m, zone i) superficially resembles flat-laminated stromatolites. However, it has several dissimilarities: (i) it lacks the common desiccation features of algal mat; (ii) fenestrae, voids and vugs are not present; (iii) banding is not due to textural

changes; (iv) thin lamination is regular. The laminated dolomicrite is also dissimilar to so-called 'cave stromatolites' reported from the Upper Proterozoic Sarnyéré Formation (Bertrand-Sarfati and Moussine-Pouchkine, 1983). The 'cave stromatolites' show pseudocolumnar growth and alternation of dolospar and detrital dolomicrite laminae.

The laminated dolomicrite of zone (i) shows certain similarities with laminar calcrete crusts known from soil surfaces or within pedogenic profiles (Multer and Hoffmeister, 1968; Walls et al., 1975; Harrison and Steinen, 1978; Arakel and McConchie, 1982; Demicco and Hardie, 1994). Similar to the studied case, the recent laminar calcretes of Australia and Florida exhibit very low porosity, laterally continuous and not fractured laminae which tend to even out irregularities on the underlying surfaces by filling depressions (Arakel and McConchie, 1982). They lack desiccation features and their bands are due to differential staining (Multer and Hoffmeister, 1968). Furthermore, the studied laminated crusts show similarities with the thin laminated calcrete crust developed on Carboniferous limestones. This is the 1–5 cm-thick crust consisting of numerous undulatory, dense calcareous laminae that generally parallel bedding, and occur as alternating light and dark coloured bands (Walls et al., 1975). However, the unconformable contacts and truncations of individual laminae, reported from the recent and Carboniferous laminated calcretes (Walls et al., 1975; Read, 1976; Harrison and Steinen, 1978; Esteban and Klappa, 1983; Wright, 1989; Demicco and Hardie, 1994), have not been observed in our case. This makes significant differences.

The colour-banded, thinly laminated dolomicrite of zone (i) shows the closest similarities to the hot-water travertine crust (Fig. 3k). The latter, however, is composed of numerous bands of 'ray crystals' and fibrous composite dolomite crystals with compromise boundaries which was the result of precipitation from hot waters (Melezhik and Fallick, 2001). Such fabrics are lacking in the colour-banded, thinly laminated dolomicrite. This is only the difference between the reported hot-water spring travertine and the colour-banded, thinly laminated micrite. However, intercalation of layers consisting of micrite and fibrous composite crystals has been reported from several recent hot-water spring deposit (Jones et al., 1996). Similarly, the laminated dolomicrite can be interpreted as a travertine crust precipitated from flowing spring water. This assertion is supported by the fact that, in several places, the colour-banded, thinly laminated dolomicrite crusts cape the hot-water travertine composed of 'ray' and fibrous composite dolomite crystals (Fig. 3f).

The nature of the red, iron-stained, non-laminated dolomicrite of zone (ii) appears to be a problem. Such structureless dolomicrite significantly differs from the background micritic and stromatolitic dolostones of the KSF. Obliteration of primary lamination of host rocks has been described to be a common feature of micritisation which occurs in soil environments (Kahle, 1997; James, 1972). However, other features of the red, non-laminated dolomicrite do not show any resemblance to those reported from any type of calcretes (e.g., Esteban and Klappa, 1983; Wright and Tucker, 1991; Demicco and Hardie, 1994). The red, iron-stained, non-laminated dolomicrite has been observed as 0.5–1 cm thick lenses filling small depressions on top of the colour-banded, laminated, travertine dolomicrite (Fig. 3p). However, the red, non-laminated dolomicrite has more dense micritic fabrics and shows more intensive staining (Fig. 3l). Tentatively, we suggest that the lack of lamination and intensive staining in the red, non-laminated dolomicrite might have been caused by its precipitation from standing body of evolved, oxygenated water in small abandoned hydrothermal pools.

The red, iron-stained, 'vuggy', non-laminated dolomicrite and dolomicrite breccia of zone (iii) possess clear features indicating solution processes. The net effect of these processes gradually decreases from the bedding surface downward (Fig. 3l and m). This indicates that vugs and microcavities have formed due to downward percolating water. Therefore, the dolospar-cemented breccia (iii) can be categorised as a dissolution breccia. The solution processes have not been observed modifying dolostone layers immediately above the dissolved surfaces, thus they have operated prior to the deposition of the overlaying sediment. The vugs, microcavities and fractures show no compaction features predating cementation, thus suggesting that the latter has been accomplished prior to burial. The dolospar cement contains only single grains of detrital quartz and a few clasts of dolomicrite indicating that the dissolved, 'vuggy' surfaces remained open and were neither infilled nor covered by sedimentary material prior to cementation. The

coated dolomicrite grains exhibit multiple pendant cement (Fig. 3l). Hence, the cementation is considered to have been accomplished in subaerial environments. This is supported by the intensive iron-staining of such dissolved surfaces, which suggests exposure to O_2-containing air. The distinctive colours such as reddish and orange, from precipitation of iron oxyhydroxides, are commonly used as an indication of soil formation (Goldstein et al., 1991).

The silicified nodular zone (Fig. 3m, zone iv; Fig. 3o) shows many similarities to the orbicular crust and oncoids of a pedogenetic alteration (calcrete) of algal boundstones described by Bertrand-Sarfati and Moussine-Pouchkine (1983) from the Upper Proterozoic Sarnyéré Formation. However, Palaeoproterozoic pedogenic caliches developed on carbonate substrate have not yet been described in the literature, therefore their recognition is problematic and provides a challenge.

Based on previous studies by many workers, Demicco and Hardie (1994 and references therein) summarised several characteristic features which have been reported to be diagnostic for relatively thin (centimetre-to-decimetre-thick), well indurated, calcrete crusts developed on Pleistocene limestones (Demicco and Hardie, 1994, p. 159). Several of these features match those described in the orbicular silicified crust (Fig. 3m–o). These are: (1) abundant dissolution microcavities and fractures filled with microdolospar cement (Fig. 3m–o); (2) pendant cement (Fig. 3n); (3) micritic glaebules, micronodules and coated grains (Fig. 3o); (4) microdolospar and dolomicrospar matrix in which the glaebules and micronodules are suspended (Fig. 3o).

The studied nodular crusts show silicification and contain silcretes and silica micronodules (Fig. 3l–o). Silica in the form of nodules and laminated chalcedonic layers is important component in many calcretes (Reeves, 1970; Walls et al., 1975; Wright and Tucker, 1991), particularly in older forms (Reeves, 1976). Silicification associated with formation of calcrete is widespread and is an integral part of the calcrete-forming processes resulting in the formation of cal-silcretes and sil-calcretes (Goudie, 1983; Summerfield, 1983).

The overall sedimentological features suggest that the vuggy dolomicrite and dolomicrite breccia were very likely produced by subaerial dissolution processes, whereas the orbicular silicified crusts show similarities with younger calcretes, and can be categorised as either superficial dolocrete or pedogenic dolocrete (e.g., Carlisle, 1983; Alonso-Zarza, 2003). Alternative explanations, such as formation by groundwaters, meet several problems, because the dolocrete crusts have formed on surfaces which were dissolved by downward percolating water (Fig. 3m). The dissolution processes did not affect the overlying beds (Fig. 3m). The open dissolution cracks and voids have been cemented by earlier isopachous, dolomicritic and multiple pendant dolomicritic cement prior to burial (Fig. 3n). The dolocrete has a limited thickness of the order of 0.5–5 cm and is not associated with any permeable horizons (Fig. 3m and n). The silicification affected the uppermost part of the dolocrete profile, and it does not modify the overlying bed (Fig. 3m and o) and thus very likely formed in the subaerial environment zone. Only the late equant dolospar, filling large voids (Fig. 3m and n), may suggest cementation below the water table. Although the pendant cement is not abundant and it is difficult to demonstrate meniscus cement, it does not necessary indicate cementation in the phreatic zone. Any preferential downwards-growth might have been obscured by later periods of cementation in the phreatic zone (e.g., Adams, 1980). Moreover, fine fabrics like meniscus and pendant cements could have been severely obliterated by metamorphic recrystallisation.

Although there are some similarities between the described dolocrete and the post-Cretaceous pedogenic calcretes, several dissimilar features are obvious. Rezolith, ‘black pebbles’, alveolar septal structures, ‘*Microcodium*’ and other fabrics associated with plant roots and input of terrestrial organic matter have not been identified. Thus, beta fabrics have not been recognised. Alfa fabrics can be applied to describe the dolocrete crusts though rhombic calcite crystals are lacking. However, a certain caution is needed while describing differences, because fine microfabrics of the dolocrete could have been obliterated by greenschist facies metamorphic processes.

Despite the limited thickness of the dolocrete crusts they are abundant in upper part of the Dolostone member implying numerous phases of the cessation of sedimentation and subaerial ‘omission surfaces’.

3.5. Silica sinters

3.5.1. Observations

Individual phases of growth observed within travertine mounds are commonly separated by internal dissolution surfaces veneered with silica sinters (Melezhik and Fallick, 2001). The upper surface of travertine crusts and mounds is always veneered with 1–5 mm-thick finely crystalline silica sinter (Fig. 3g, h and q). The lower contact of the silica sinter has a corrosive relationship with the travertine dolomite (Fig. 3s). It may be a series of 1–2 mm thick silica sinters deposited on top of the travertine crust and mound. Some of them show 'V'-shaped desiccation cracks, in situ fragmentation and separation by 0.1–0.5 mm thick laminae of red and brownish, hematite-rich, mudstone (Fig. 3r). Where travertine mounds were partly eroded, the outer silica sinter is also removed.

3.5.2. Interpretation

The relationship between travertines, silica sinters and overlaying rocks of the KSF (Fig. 3r) suggests that silicification occurred prior to burial. Intercalation of desiccated and fragmented silica sinters with thin films of red, hematite-rich mud on top of the travertine crusts is consistent with subaerial precipitation of SiO_2 when there was no carbonate deposition and a limited input of clastic material, mainly in the form of fine particles of clay and hematite apparently blown by wind. Shrinkage structures in silica sinters and cherts formed in similar environments have been reported from the Lake Magadi basin in the Kenya Rift Valley (Behr, 2002).

3.6. Travertine

3.6.1. Observations

The travertine is abundant in the Dolostone Member. It occurs in the form of crusts and small-scale mounds as well as veins representing feeder zones (Fig. 3s and t). The traverine crusts and mounds have been described in detail by Melezhik and Fallick (2001) who categorised them as autochthonous hot-water spring travertine.

In places, travertine dolomite covers a very irregular microrelief above beds containing abundant laminoid voids (Figs. 3h and s). The voids and fractures extend from the bedding surface downwards over a distance of 5–20 cm. Although their orientation is variable, there are often vague subhorizontal (bedding-parallel) aspects to the majority of these voids and fractures on both macroscopic and microscopic scales. Fractures may also show a cross-cutting relationship and form an irregular network. Both the voids and the fractures are walled and filled with travertine dolomite. This results in the development of macro-clotted fabrics which significantly modify the structure of primary dolostones (Fig. 3s).

3.6.2. Interpretation

The presence of travertines in the Dolostone Member signifies a non-marine depositional system because modern and ancient travertines have been only reported in subaerial environments (e.g., Demicco and Hardie, 1994). The hot-water spring travertines occur in the Dolostone Member as a stack of numerous crusts (Fig. 3t), thus indicating that a subaerial environment prevailed during deposition of ^{13}C-rich host dolostones and that there were numerous exposure surfaces. Irregular micro-surfaces associated with laminoid vugs suggest that episodes of emergence were also marked by partial dissolution of the dolomite.

4. Geochemistry

4.1. Methods

The geological material was studied petrographically and analysed by various analytical techniques. In situ analyses of carbonate minerals were performed by using EMP and LA-ICP-MS instruments. The measurements were carried out at the Earth Science Department of the University of Bristol. Concentration of Mg and Ca were measured on a Microprobe Jeol JXA 8600 instrument equipped with wavelength dispersive (WD) and energy dispersive (ED) spectrometers. The operating conditions were as follows: take-off angle 40°, acceleration voltage 15 kV, beam current 15 nA, beam diameter 10 μm, working distance 11 mm. The following calibration standard references have been used: calcite (10) for Ca, dolomite (14) for Mg, magnetite (26) for Fe, bustamite (9) for Mn. Numbers in parenthesis refer to the reference sample number. De-

tection limit for Ca and Mg is 0.1 wt.% (wavelength dispersive spectrometer).

Concentration of Fe, Mn, Sr and Ba were measured on a LA-ICP-MS. The analytical precision is 10% (1σ) for high concentration elements (>50 ppm) and 20% for lower concentration (<10 ppm), and the precision is almost invariably higher than the accuracy.

Submilligram microsamples for oxygen and carbon isotope analyses were obtained using a Ulrike Medenbach microcorer. The microsamples were cored from 150 μm thick polished sections. The microcores were obtained from the spots which were analysed in situ for major and trace elements. Oxygen and carbon isotope analyses of microcores were carried out at Scottish Universities Environmental Research Centre using the phosphoric acid method of McCrea (1950) modified for operation at 90 °C with a VG PRISM + ISOCARB mass spectrometer. Oxygen isotope data were corrected using the fractionation factor 1.00932 recommended by Rosenbaum and Sheppard (1986) for dolomites. The δ^{13}C data are reported in per mil (‰) relative to V-PDB and the δ^{18}O data in ‰ relative to V-SMOW. Calibration to international reference material was through NBS 19 and precision and accuracy for isotopically homogeneous material is better than ±0.1‰ (1σ).

4.2. Major and trace element geochemistry

Thirty-six in situ measurements of Mg, Ca, Sr, Ba, Fe and Mn concentrations have been obtained from carbonate rocks which were affected by dissolution processes (Tables 1 and 2). Ninety-five ICP-AES (acid-soluble) analyses of Mg, Ca, Sr, Fe and Mn from the KSF dolostones and 24 electron-probe microanalyses from the travertine have been incorporated from our earlier work (Melezhik and Fallick, 1996, 2001) for comparison.

The stratified carbonate rocks of the KSF, as well as the travertine crusts, are composed of dolomite. Based on whole-rock analyses, an average MgO/CaO ratio of the stratified dolostones is 0.67 which is slightly lower

Table 1
Isotopic profiles through dolocrete and its substrate in the drillcore obtained from DH X

Sample nn[a]	CaO[b] (wt.%)	MgO[b] (wt.%)	CO_2 (wt.%)	Total (wt.%)	$CaCO_3$[c] (mol%)	$MgCO_3$[c] (mol%)	MgO/CaO	Mn[d] (ppm)	Fe[d] (ppm)	Sr[d] (ppm)	Ba[d] (ppm)	δ^{13}C (‰ V-PDB)	δ^{18}O (‰ V-SMOW)
Dolocrete and its substrate in the drillcore obtained at depth of 269.5 m, Fig. 5a													
Dolocrete													
Equant dolospar cementing vugs and fractures in iron-stained dolomicrite													
19	31.6	20.2	46.9	98.7	52.9	47.1	0.64	952	99	564	2.7	+6.6	15.6
18	31.7	20.3	47.0	99.0	52.8	47.2	0.64	221	218	282	2.7	+6.7	16.4
17	32.8	19.8	47.3	99.9	54.4	45.6	0.60	372	283	372	3.4	+6.7	16.2
14	n.d.	n.d.	n.d.	n.d.	n.d.	n.d.	n.d.	n.d.	n.d.	n.d.	n.d.	+6.6	15.6
Red, iron-stained, non-laminated, 'vuggy' dolomicrite													
21	31.8	20.1	46.9	98.7	53.2	46.8	0.63	714	1205	469	51	+6.8	16.3
20	33.1	19.6	47.4	100.2	54.8	45.2	0.59	812	1384	527	92	+6.5	15.4
16	32.2	20.1	47.2	99.4	53.6	46.4	0.62	1040	1536	588	90	+6.6	15.5
15								n.d.	n.d.	n.d.	n.d.	+6.7	15.8
13	31.2	21.0	47.4	99.6	51.7	48.3	0.67	1123	3116	577	320	+6.7	14.7
12	n.d.	n.d.	n.d.	n.d.	n.d.	n.d.	n.d.	n.d.	n.d.	n.d.	n.d.	+6.6	14.8
Dolostone substrate													
'Cloudy' dolomicrite													
11	31.0	20.5	46.7	98.2	52.1	47.9	0.66	649	833	546	18	+6.6	15.0
10	31.4	20.4	46.9	98.6	52.5	47.5	0.65	626	568	518	3.4	+6.6	15.9
Dolostone substrate													
'Cloudy' dolomicrite													
9	31.6	20.6	47.4	99.7	52.4	47.6	0.65	635	590	588	3.2	+6.6	15.1
6	31.5	20.7	47.3	99.6	52.2	47.8	0.66	676	637	507	5.6	+6.4	15.4
5	31.3	20.6	47.0	98.8	52.2	47.8	0.66	588	586	524	2.5	+6.2	15.0
4	31.5	20.3	46.9	98.7	52.8	47.2	0.64	794	729	591	6.7	+6.4	15.3
3	31.5	20.4	47.0	98.9	52.6	47.4	0.65	464	492	443	2.8	+5.9	11.3

Table 1 (*Continued*)

Sample nn[a]	CaO[b] (wt.%)	MgO[b] (wt.%)	CO_2 (wt.%)	Total (wt.%)	$CaCO_3$[c] (mol%)	$MgCO_3$[c] (mol%)	MgO/CaO	Mn[d] (ppm)	Fe[d] (ppm)	Sr[d] (ppm)	Ba[d] (ppm)	$\delta^{13}C$ (‰ V-PDB)	$\delta^{18}O$ (‰ V-SMOW)
Beige dolomicrite													
8	31.3	20.6	47.0	98.8	52.2	47.8	0.66	488	661	400	10	+6.4	13.6
7	31.7	20.2	46.9	98.8	53.0	47.0	0.64	535	596	406	12	+6.6	15.2
Sandy dolostone													
2	31.4	20.3	46.8	98.5	52.6	47.4	0.65	787	453	113	3.0	+6.3	13.7
1	31.1	20.6	46.9	98.7	52.0	48.0	0.66	313	242	298	2.9	+5.9	15.9
Caliche zone in the drillcore obtained at depth of 310 m, Fig. 5b													
Dolocrete													
Suspended, nodular dolomicrite and dolomicrosparite													
26	30.3	21.9	47.8	100.0	49.8	50.2	0.72	36	283	187	1.6	+8.2	22.0
25	31.2	21.6	48.1	100.9	50.9	49.1	0.69	29	285	144	1.1	+7.4	19.8
Dolocrete													
Suspended, nodular dolomicrite and dolomicrosparite													
24	31.0	21.8	48.1	100.9	50.5	49.5	0.70	23	225	151	1.8	+6.7	19.5
23	30.9	21.6	47.8	100.3	50.7	49.3	0.70	21	223	156	1.2	+7.4	29.5
22	30.7	21.9	48.0	100.6	50.2	49.8	0.71	67	590	196	1.0	+7.2	19.7
Equant dolospar cementing vugs and fractures in iron-stained dolomicrite													
20	n.d.	n.d.	n.d.	n.d.	n.d.	n.d.	n.d.	n.d.	n.d.	n.d.	n.d.	+8.2	22.6
19	30.6	21.5	47.5	99.6	50.6	49.4	0.70	39	454	147	0.3	+7.1	20.2
10	30.4	21.8	47.7	99.9	50.0	50.0	0.72	8.1	135	34	0.4	+6.9	19.9
Red, iron-stained, 'vuggy', non-laminated dolomicrite													
21	30.8	21.7	47.9	100.4	50.5	49.5	0.70	81	1837	219	92	+7.3	20.0
18	30.6	21.8	47.8	100.2	50.2	49.8	0.71	79	2109	222	110	+6.8	20.4
17	30.4	21.5	47.3	99.2	50.4	49.6	0.71	71	1022	220	45	+7.3	26.7
16	n.d.	n.d.	n.d.	n.d.	n.d.	n.d.	n.d.	n.d.	n.d.	n.d.	n.d.	+7.5	21.5
15	30.6	21.6	47.6	99.8	50.5	49.6	0.71	54	1578	233	89	+7.2	19.9
14	n.d.	n.d.	n.d.	n.d.	n.d.	n.d.	n.d.	n.d.	n.d.	n.d.	n.d.	+7.5	20.4
13	30.5	21.4	47.3	99.2	50.6	49.4	0.70	53	1163	237	54	+7.4	20.7
12	30.5	21.7	47.6	99.8	50.3	49.7	0.71	92	1805	213	91	+6.7	17.3
Travertine crust													
Colour-banded, laminated dolomicrite													
11	n.d.	n.d.	n.d.	n.d.	n.d.	n.d.	n.d.	n.d.	n.d.	n.d.	n.d.	+1.8	14.8
9	30.4	21.5	47.3	99.2	50.4	49.6	0.71	86	839	209	19	+6.9	19.2
8	30.5	21.6	47.5	99.6	50.4	49.6	0.71	86	648	213	16	+6.4	18.5
7	n.d.	n.d.	n.d.	n.d.	n.d.	n.d.	n.d.	n.d.	n.d.	n.d.	n.d.	+7.2	20.0
6	n.d.	n.d.	n.d.	n.d.	n.d.	n.d.	n.d.	n.d.	n.d.	n.d.	n.d.	+6.9	21.2
5	n.d.	n.d.	n.d.	n.d.	n.d.	n.d.	n.d.	n.d.	n.d.	n.d.	n.d.	+2.6	27.0
3	30.3	21.5	47.3	99.1	50.3	49.7	0.71	116	1751	192	71	−3.6	8.9
Substrate to travertine													
Sandy, sparry dolostone													
4	n.d.	n.d.	n.d.	n.d.	n.d.	n.d.	n.d.	n.d.	n.d.	n.d.	n.d.	+7.3	20.4
2	30.7	21.9	48.0	100.6	50.2	49.8	0.71	63	551	172	2.6	+7.6	21.5
1	30.5	21.4	47.3	99.2	50.6	49.4	0.70	77	524	167	5.4	+7.6	20.8

n.d.: not determined.

[a] Analysis points as shown in Fig. 5a and b.

[b] Values measured in situ by using EMP instrument.

[c] Calculated values.

[d] Values measured in situ by using LA-ICP-MS instrument.

Table 2
Isotopic profile through the dolocrete in the drillcore obtained at a depth of 278.0 m (Fig. 5c).

Sample nn[a]	δ^{13}C (‰ V-PDB)	δ^{18}O (‰ V-SMOW)
Overlying sandy, dolomicrite		
17	+7.2	19.8
16	+7.2	17.3
15	+7.3	16.1
Dolocrete		
Equant dolospar filling vugs and fractures		
11	+7.5	17.7
10	+7.2	17.8
6	+6.5	16.0
3	+7.0	19.0
Suspended, nodular dolomicrite		
14	+7.2	18.8
12	+6.7	15.2
9	+7.2	17.0
8	+8.1	17.5
7	+7.1	16.7
5	+7.3	17.9
4	+7.1	17.1
2	+7.1	17.6
1	+6.9	18.3

n.d.: not determined.
[a] Analysis points as shown in Fig. 5c.

than in stoichiometric dolomite (0.72). The stratified dolostones are relatively low in Mn (360 ppm on average, $n = 95$) and relatively rich in Sr (174 ppm, $n = 95$). Electron-probe microanalyses show similar MgO/CaO ratios spanning 0.64–0.71, whereas Mn, Fe and Sr concentrations span 60–800, 240–830 and 110–600 ppm, respectively. The rocks have low Ba concentration, 2.5–18 ppm (Table 1).

Based on electron-probe microanalyses, the MgO/CaO ratio of the travertine dolomite is approximately 0.70. Mn, Fe and Sr abundances span 90–120, 650–1650, and 190–210 ppm, respectively (Table 1). The Ba content ranges between 15 and 70 ppm.

The electron-probe microanalyses show that the 'vuggy' rocks and their later infills from dissolution surfaces have dolomitic composition with MgO/CaO ratios fluctuating between 0.60 and 0.72 (Table 1). The red, iron-stained, 'vuggy', non-laminated dolomicrite (Fig. 3h and i) is enriched in Fe (1000–3100 ppm) and Ba (45–320 ppm) compared with similar red, iron-stained dolomicrite unaffected by dissolution (Fe = 500–800, Ba = 2.5–18 ppm, Table 1). The late dolospar, cementing vugs and fractures, is slightly depleted in Fe and Ba and rather similar in Mn, and Sr concentrations to the stratified dolomite and travertine dolomite which were not affected by dissolution processes (Table 1).

4.3. Carbon and oxygen isotopes

Sixty-three microcored samples obtained from the carbonate rocks affected by dissolution processes have been analysed for carbon and oxygen isotopes (Tables 1 and 2). Thirty-five carbon and oxygen isotope analyses of the KSF dolostones and 29 analyses of the travertine have been incorporated from our earlier work (Melezhik and Fallick, 1996, 2001) for comparison. The KSF dolostones have δ^{13}C and δ^{18}O ranging between +6.6 and +7.6‰ (average $+6.9 \pm 0.7$‰, $n = 35$), and 16.7–21.5‰ (average 16.7 ± 2.2‰), respectively (Melezhik and Fallick, 1996). In contrast, microcored samples of travertine dolomite exhibit δ^{13}C and δ^{18}O values ranging from –6.1 to +7.7‰ and 12.0 to 21.5‰, respectively (Melezhik and Fallick, 2001).

The immediate substrate on which the red, non-laminated dolomicrite and 'vuggy' dolomicrite were developed is represented by sandy dolostone with $\delta^{13}C_{dol}$ and $\delta^{18}O_{dol}$ values of around +7.5 and 21‰, respectively (Table 1); and by colour-banded, laminated travertine dolomite (zone i) with δ^{13}C clustering between −3.6 and +7.2‰, whereas δ^{18}O exhibits a larger range, 8.9–27.0‰ (Table 1). This range is in agreement with our previous study (Melezhik and Fallick, 2001) which demonstrated that the travertine dolomites and background stratified dolostones of the KSF plot along two entirely different trend lines which converge (Fig. 4). δ^{13}C and δ^{18}O values of the travertine dolomite are characterised by a strong positive correlation, whereas the stratified dolostones exhibit insignificant δ^{13}C–δ^{18}O correlation. The best fit line is essentially parallel to the δ^{18}O axis, whereas for the travertine samples the gradient is 0.6 (Melezhik and Fallick, 2001).

The iron-stained, 'vuggy', non-laminated dolomicrite, the nodular dolomicrite and the late equant dolospar show a similar δ^{13}C range. A few samples are marked by elevated δ^{18}O (up to 29.5‰) (Fig. 4). All these dolomite phases plot along a horizontal line which is slightly different from the one representing the substrate dolomite (Fig. 4). Three separate profiles through the dolocrete selected for the isotopic

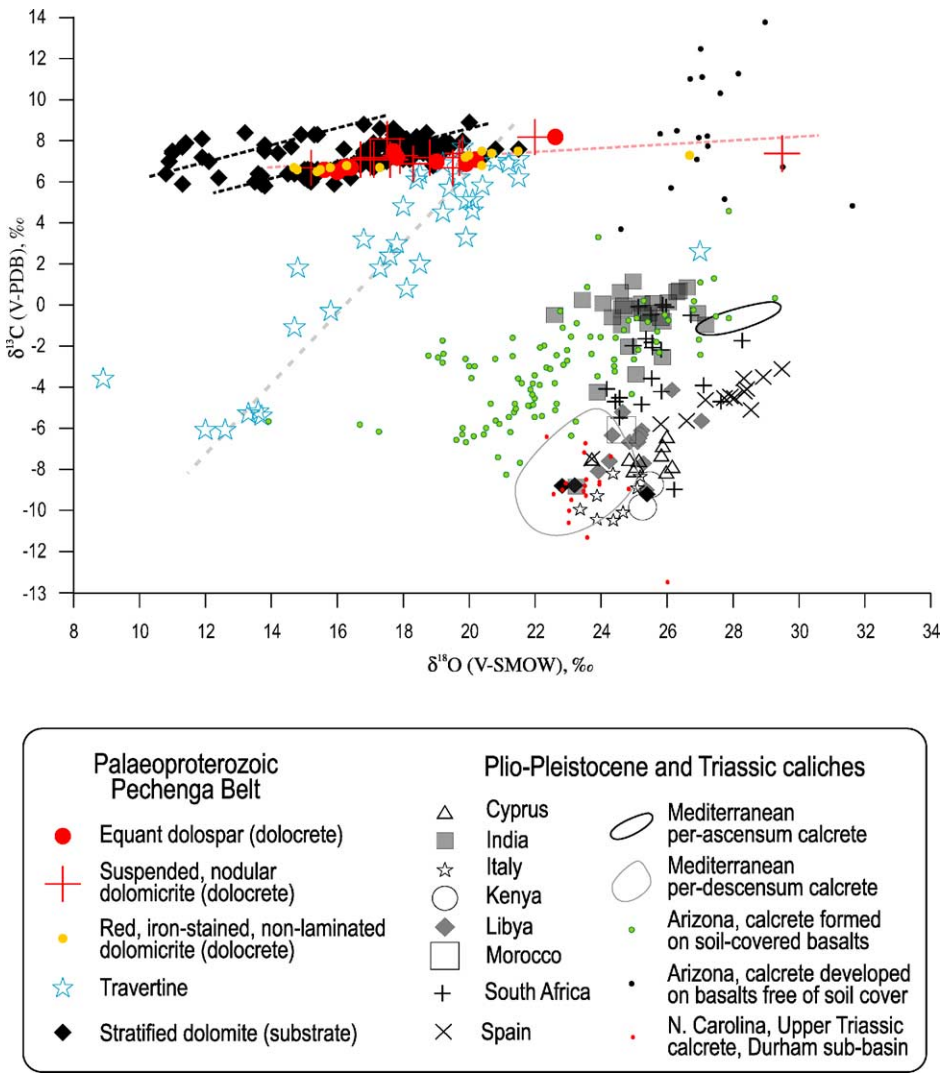

Fig. 4. $\delta^{13}C_{carb}$ vs. $\delta^{18}O$ plot showing that substrate dolomite and caliche dolomite plot along slightly different trajectories whereas travertine dolomites plot along and entirely different regression line. The isotopic composition of Plio-Pleistocene caliches shown for comparison. Data for Arizona caliche are from Knauth et al. (2003); data for other Plio-Pleistocene caliches are from Salomons et al. (1978) and Manze and Brunnacker (1977); data for Late Triassic calcrete are from Driese and Mora (2002).

study differ slightly from each other with respect to $\delta^{13}C$ and $\delta^{18}O$ values; however, none of them reveals systematic variations of $\delta^{13}C$ and $\delta^{18}O$ (Fig. 5).

4.4. Diagenetic and metamorphic overprint of oxygen and carbon isotope systems

Change in oxygen and carbon isotope compositions during diagenesis and metamorphism strongly depends on water to rock ratio (η) for both closed and open system interaction. Oxygen isotopes are commonly easily affected by exchangeable oxygen derived from either meteoric water or interstitial fluids at elevated temperatures (e.g., Fairchild et al., 1990), whereas original $\delta^{13}C$ variations may be largely preserved because they are buffered by pre-existing carbonate due to the low water/rock ratio for C in later fluids (e.g., Banner and Hanson, 1990). In general, η

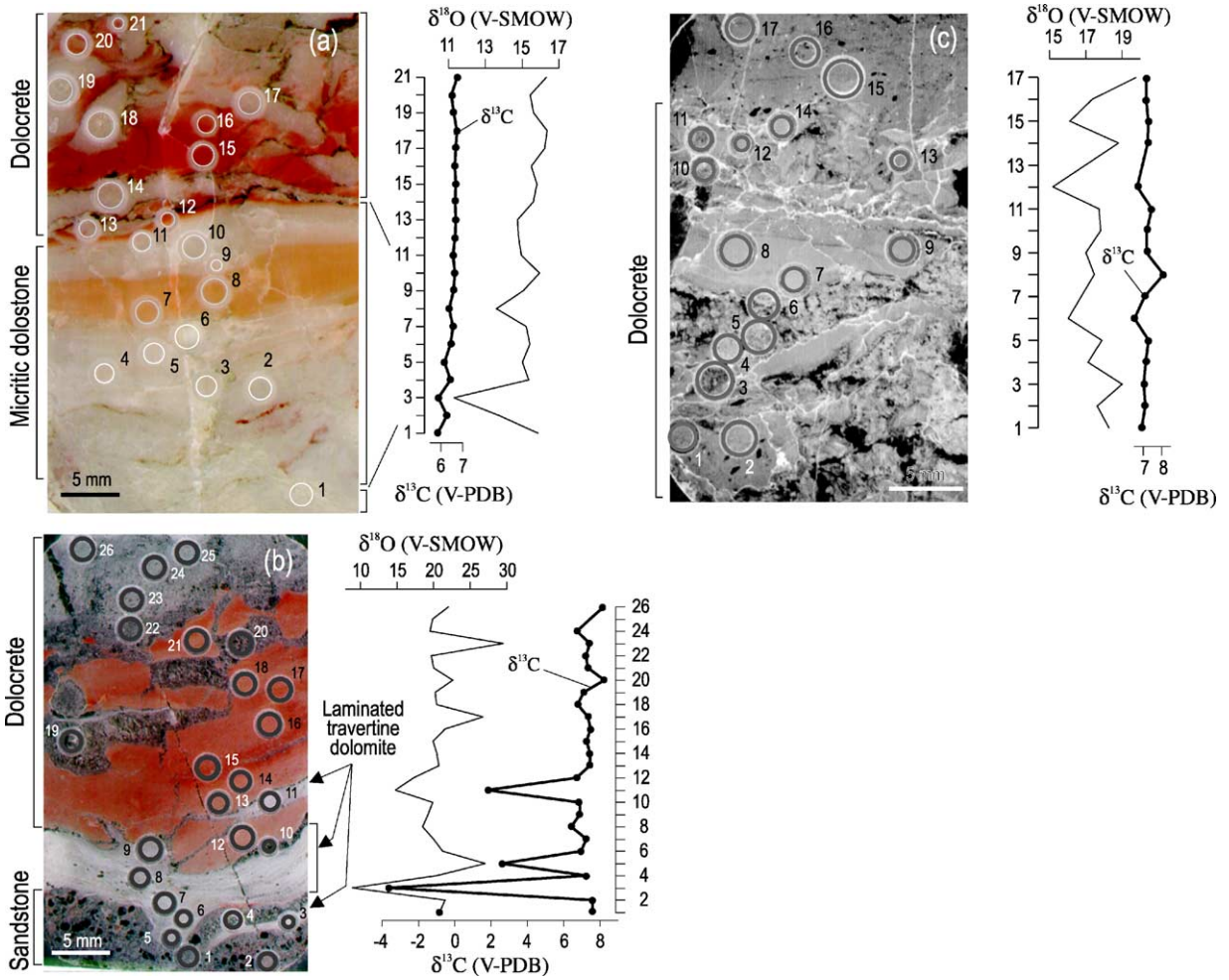

Fig. 5. Isotopic profiles through thin dolocrete crusts. (a) Substrate to dolocrete consists of white (1–6, 9–11) and pale orange, iron-stained (7–8) dolomicrite. The dolocrete (12–21) is composed of in situ brecciated, red, iron-stained, non-laminated dolomicrite (12, 15, 16, 20, 21) cemented with earlier dolomicrite and filled with late equant dolospar (13, 14, 17). Microcores 18 and 19 are obtained from coated dolomicrite grain. Circles represent microcored samples. Scanned image of thin section. Sample is from DH X, depth 269.5 m (Fig. 2); the upper part of the Dolostone Member. (b) Substrate to dolocrete consists of dolomite-cemented sandstone (1, 2, 4) veneered by laminated travertine crust (5–9). The dolocrete is composed of silicified nodular zone (22–26), and vuggy, iron-stained, non-laminated dolomicrite (21), developed on fractured, iron-stained, non-laminated dolomicrite (12–18). Late equant dolospar fills large voids (19–20) and some fractures (10). Note thin lamina of travertine in the sandstone (3) and in the red dolomicrite (11). Scanned image of thin section. Sample is from DH X, depth 310.0 m (Fig. 2); the middle part of the Dolostone Member. (c) Scanned image of thin section illustrating cross-section through the dolocrete consisting of (1) in situ brecciated, non-laminated dolomicrite (1, 2, 7, 8, 9, 12, 14): (2) dissolution cavities filled with equant dolospar (3, 10, 11) and silica (black); and (3) nodular dolomicrite (5, 6) suspended in dolomicritic cement (4, 6). The dolocrete is covered with dolarenite (15–17). Sample is from DH X, depth 278.0 m (Fig. 2); the upper part of the Dolostone Member.

required for $\delta^{13}C$ to be totally equilibrated with the fluids is an order of magnitude higher as compared to that of $\delta^{18}O$ (e.g., Jacobsen and Kaufman, 1999).

This general consideration is in agreement with the focused studies of diagenetic (Melezhik and Fallick, 2003) and metamorphic (Melezhik et al., 2003) overprints of the KSF dolostones. In the low-grade greenschist facies conditions, distinct textural components from the same parental impure dolostones have yielded $\delta^{13}C$ values ranging within 1‰. Genetically

different dolomites, however, retain their primary isotopic signatures which is also demonstrated by Fig. 4 (e.g., stratified dolostones versus travertines). The $\delta^{13}C$ and $\delta^{18}O$ values of the travertine dolomites are characterised by a strong positive correlation which a characteristic feature of many travertine-depositing hot springs (Gonfiantini et al., 1968; Friedman, 1970; Chafetz and Lawrence, 1994; Guo et al., 1996; Fouke et al., 2000).

In contrast, $\delta^{18}O$ values of the stratified dolostones show up to a 6‰ range associated with diagenetic/metamorphic resetting (Melezhik et al., 2003; Melezhik and Fallick, 2003). Partial resetting of the oxygen isotopes resulted in an O/C trend paralleling the oxygen axis (Fig. 4).

5. Discussion

Various subaerial exposure features described in Section 3 suggest that the depositional site experienced numerous phases of emergence and was frequently exposed to the air, consequently resulting in numerous 'omission surfaces'. In general, subaerial exposure surfaces can result from (i) uplift, (ii) eustatic fall in sea level, and (iii) vertical aggradation of sediment into the subaerial realm without uplift or eustatic fall (e.g., Goldstein et al., 1991). The focused sedimentological study of the KSF (Melezhik and Fallick, in press) does not suggest shoaling-upwards sequence and therefore vertical aggradation processes should not be considered as the cause of emergence. The limited geological data do not allow us to discriminate between the other two causes. However, whatever the cause, what is crucially important is that the frequent exposures should create decoupling between the Kuetsjärvi basin and neighbouring open sea, supposing that such a sea existed. Unfortunately, the duration of episodes without sedimentation remains unknown.

5.1. Origin and source of dolocrete-forming carbonate solutions

Numerous mechanism have been proposed for the origin of calcrete materials. Bretz and Horberg (1949 and references therein), who critically reviewed these theories, acknowledged that it is unlikely that any one theory listed below is of general application: (1) deposition in extensive shallow lakes by algae and inorganic processes; (2) deposition in small disconnected lakes and ponds by physical and/or organic processes; (3) deposition along streams by physical and/or organic processes; (4) deposition by rising artesian waters either at the water table or at the surface; (5) deposition by capillary rise of water from the water table, especially under conditions of high water table; (6) deposition in the *B* zone of the soil profile by descending surface waters (per-descensum calcrete) or by capillary rise of surface waters (per-ascensum calcrete) following saturation of the soil zone.

Each of these mechanisms could be applied to the Kuetsjärvi dolocretes. The fluvial hypothesis (3) is very unlikely as rimstone tufa and calcareous encrustations were not observed. The lacustrine hypotheses (1 and 2) could be applicable to the Kuetsjärvi dolocretes in the sense that they developed on lacustrine dolostones. There remains, however, the question of the presence of algal structures: they were not observed, although metamorphic overprint could have obliterated them.

The pedogenic hypothesis (6) is not consistent with the features described, only in the sense that Recent type of soil profiles, including A, B and C horizons, were not observed in the Palaeoproterozoic. However, several lines of evidence discussed above suggest the dolocretes studied do represent surface phenomena.

In general, calcretes could be formed by the precipitation of carbonate minerals in the phreatic, vadose, pedogenic zones and on the surface. As gravitational cement is not abundant in the case studied, the precipitation of dolocrete from downward-percolating meteoric water should have been limited. This mechanism is also not supported by isotopic signatures of the dolocrete. Meteoric water commonly results in low values for both $\delta^{18}O$ and $\delta^{13}C$ (and at least the former would be expected) which were not documented. In contrast, the opposite $\delta^{18}O$ trend has been observed in the dolocrete (Fig. 4). Thus, it is very likely that the dolocrete was precipitated from films of pore water which was brought up to the surface by capillary draw and evaporation pumping (per-ascensum calcrete). This is somewhat similar to formation of calcrete on pre-existing Cretaceous limestones by downward leaching and upward movement of carbonate (Blank and Tynes, 1965). In general, the source of pore water could be superficial rainwater, soil (regolith) water or

perennial groundwater (e.g., Carlisle, 1983; Demicco and Hardie, 1994). The perennial groundwater was one probable source of pore water as indicated by the presence of tepees in the KSF (Melezhik and Fallick, in press). Abundant subaerial exposure and subaerial dissolution surfaces suggest that diluted rainwater from episodic rainfalls, percolating downwards under gravity, was another source. However, subaerial dissolution features associated with surface meteoric water have very limited development. This suggests that the volume of rainwater was rather restricted. Regolith water, percolating meteoric water and groundwater were likely enriched in calcium bicarbonate as they drained the dolostone-dominated environment. During dry seasons, under the driving force of evaporative pumping (e.g., Hsu and Siegenthaller, 1969), these waters were transported upwards back to the surface where the evaporation resulted in the precipitation of the superficial dolocrete, apparently in the regolith zone.

5.2. Carbon and oxygen isotope composition of dolocretes and their carbonate substrate

C and O isotope analyses of whole-rock and microcomponent samples are commonly used to identify ancient surfaces of subaerial exposure (Allan and Matthews, 1982; Goldstein et al., 1991; Cander, 1995; Dickson and Saller, 1995; Wagner et al., 1995). Allan and Matthews (1982) suggested that marine carbonates during subaerial exposure could produce a relatively negative $\delta^{13}C$ signal from plant-derived soil-gas CO_2, a relatively positive $\delta^{18}O$ value from evaporation, and an overall shift in $\delta^{18}O$ because of different diagenetic histories across a buried surface of subaerial exposure. However, in general, $\delta^{13}C$ can be influenced by several factors including amount of decomposing organic matter, fractionation during degassing of CO_2, and the contribution of sedimentary and atmospheric carbon (Fornaca-Rinaldi et al., 1968; Hendy, 1971; Cerling et al., 1989). Variation in $\delta^{18}O$ might be related to the isotopic composition of meteoric water, temperature, kinetic factors, evaporation, and degree of preservation of the original sediment signal (Fantidis and Ehhalt, 1970; Salomons et al., 1978). Finally, subsequent diagenesis and metamorphism can overprint an isotopic signal associated with the exposure event.

The KSF dolomites on which dolocretes developed exhibit ^{13}C enrichment (Fig. 4). As discussed in a series of previous publications the formation of ^{13}C-rich dolostones is associated with the global 2400–2060 Ma positive excursion of carbonate $^{13}C/^{12}C$ which was driven by perturbation of the global carbon reservoir (Baker and Fallick, 1989a,b; Karhu, 1993). There are apparent isotopic similarities between the dolocrete and substrate dolomite in the KSF, though a few dolocrete samples show high $\delta^{18}O$ values (Fig. 4) despite diagenetic and metamorphic resetting of the oxygen isotopes towards lower values (Melezhik et al., 2003; Melezhik and Fallick, 2003).

Previous isotopic studies of Plio-Pleistocene calcretes show that $\delta^{13}C$ values of pedogenic carbonates range between −13 and +1‰ (Fig. 4, Manze and Brunnacker, 1977; Salomons et al., 1978; Driese and Mora, 2002). These values are broadly in agreement with carbonate precipitated from soil solutions which derive their carbon from soil CO_2 dominated by vegetation and from atmospheric carbon dioxide. Notably, an isotopic difference has been observed between carbonates precipitated by upward moving (−1 to 0‰) and downward percolating (−11 to −5‰) solutions in the same area (Fig. 4, Manze and Brunnacker, 1977). This apparently suggests that the per-descensum calcrete obtained carbon from soil CO_2 whereas the per-ascensum calcrete derive their carbon from underlying marine limestones.

Knauth et al. (2003) reported a significant difference in isotopic composition of calcretes developed on soil and soil-free environments in basaltic terrains. The calcretes formed within soil are depleted in ^{13}C and ^{18}O and show an isotopic similarity with other Plio-Pleistocene calcretes (Salomons et al., 1978; Manze and Brunnacker, 1977). In contrast, the calcrete developed directly on soil-free basalt surfaces show considerable enrichment in both ^{13}C and ^{18}O (Fig. 4). A convincing combined evaporative-biological mechanism was invoked to explain high $\delta^{13}C$ and $\delta^{18}O$ in these calcretes developed directly on soil-free basalt surfaces (Knauth et al., 2003).

The KSF dolocretes show a clear isotopic similarity to Plio-Pleistocene per-ascensum calcrete formed on a carbonate substrate in that they do not show any significant difference in C isotopic composition with respect to substrate from which the source of carbonate derived, yet they exhibit enrichment in ^{18}O, apparently caused by evaporation. Presumably, then, the KSF dolocretes were precipitated on the surface

(regolith) due to evaporation of capillary water. Because of the absence of ^{13}C-depleted values in the KSF dolocretes, the source largely lacked ^{12}C-rich carbonate derived from soil or from other C_{org}-rich sources enriched in ^{12}C. Preferential accumulation of ^{13}C has not been documented in the dolocrete studied; therefore, there was apparent lack of biological uptake of ^{12}C combined with the evaporation. Thus, the biological mechanism involved in ^{13}C enrichments of calcretes, e.g. as reported by Knauth et al. (2003) for calcrete developed on soil-free basalts, is not documented in the KSF dolocretes. Moreover, there is no isotopic indication that that ^{12}C-rich CO_2 derived from degradation of C_{org}-rich material similar to Recent soils, was incorporated into dolocretes.

5.3. Dolomite

Although dolomite is not very extensively developed in Plio-Pleistocene caliche (Goudie, 1973), several reports acknowledge abundant dolomite filling cavities and fractures in some calcite profiles (Hay and Leeder, 1978). Dolocretes were found to be more prevalent in areas where groundwater salinity is elevated (Mann and Horwitz, 1979).

However, dolomite is a common component of ancient lacustrine carbonates. Such dolomite is typically attributed to elevated salinity in the depositional environment as well as to later groundwater alteration of lacustrine limestones during periods of subaerial exposure (Wolfbauer and Surdam, 1974; Freytet, 1973). Importantly, dolomite is found in much greater abundances in Precambrian rocks than in modern carbonate environments. Tucker (1982), based on petrographic and isotopic evidence, suggested that in Precambrian time dolomite was the principal carbonate mineral precipitated from seawater and during early diagenesis.

Melezhik and Fallick (2001) reported that Palaeoproterozoic travertines, as well as all background carbonate sedimentary rocks of the KSF, are also entirely composed of dolomite. Moreover, a general lack of replacement textures in the travertines allows the consideration of dolomite as a principal carbonate mineral that was precipitated from water with a high Mg/Ca ratio (Melezhik and Fallick, 2001). The Kuetsjärvi dolocretes provide no exception as they are also entirely composed of dolomite. Thus, similar factors could be suggested to govern the dolomite precipitation in travertines, substrate dolostones and dolocretes. In accordance with earlier studies of Precambrian dolomite (e.g., Tucker, 1982), and of the KSF dolostones and travertines (Melezhik and Fallick, 2001)—as well as with the discussion presented in the previous section—the dolocrete was very likely precipitated from solutions with an elevated Mg/Ca ratio. The latter was apparently largely buffered by the substrate dolomite.

5.4. Silcretes

Chert nodules and laminated chalcedonic layers (silcretes) are common in most calcrete profiles (Reeves, 1970; Walls et al., 1975; Goudie, 1983; Summerfield, 1983). Silicification associated with calcretisation is widespread and may be an integral part of pedogenic processes (Goudie, 1983) under certain climatic conditions, as silcretes (similarly to calcretes) form in arid to semi-arid regions (Blatt et al., 1980; Summerfield, 1983). In per-descensum calcrete profiles silica layers are mainly confined to the lower parts of the profile (Reeves, 1970). However, concentration of silica in the lower levels of calcrete profiles is far from universal (Goudie, 1983).

Silica cements associated with unconformities have been described in many carbonate platforms (e.g., Meyers, 1977). In general, petrographic observations indicate the following sequence of events: (i) carbonate dissolution, (ii) precipitation of silica microspherules, (iii) precipitation/carbonate replacement by crystalline megaquartz with inclusions, (iv) precipitation/carbonate replacement by crystalline micro- and megaquartz, and (v) chertification of fine-grained carbonate lithologies.

In the KSF case, the silicification occurs in the form of silica micronodules and silica cement replacing dolomite in the uppermost surface of the dolocrete (Fig. 3m–o). Therefore, similarly to the younger counterparts, these silica phases can be termed as silcrete. The relationship between the silcrete and subaerial exposure surfaces in the KSF suggests that silica was transported upwards and precipitated on the surface. In general, lakes in rifts with volcanic rocks in their catchments commonly have waters rich in silica (Ashley and Renaut, 2002). The alternative silica source is considered to be underlying quartz-bearing dolostones from which silica could have been

mobilised and dissolved in highly alkaline ground water. The very alkaline nature of the solution allows periodic supersaturation by silica (H_4SiO_4) in exchange for carbonate. In dry climatic conditions, silica saturated solutions were apparently transported vertically by a mechanism of capillary rise and precipitated on the surface either by evaporation or by mixing with meteoric water (e.g., Summerfield, 1983; Smale, 1973; Mutti, 1995).

5.5. Significance of dolocretes and silcretes

The dolocretes and silcretes studied are of significance because they indicate several episodes of subaerial exposure, erosion and the cessation of sedimentation. The cessation of sedimentation was apparently associated with temporal uplifts and reconfiguration within the rift system. The time required to develop calcrete deposits is not well established (Alonso-Zarza, 2003). The Pleistocene calcrete on Barbados, formed on marine limestones, has rates of net accumulation of 0.6–3 cm/1000 years (James, 1972). Radiocarbon dates by Robbin and Stipp (1974) on thin Holocene laminated crusts on the Florida Keys indicate crust accretion of about 3.5 cm/1000 years. At such rates, a series of 0.5–5 cm-thick dolocretes developed in the KSF suggests several phases of emergence, each lasting up to of the order of a thousand years.

Calcretes and silcretes, in general, appear to be a world-wide feature of arid and semiarid regions (Bretz and Horberg, 1949; Reeves, 1970; Summerfield, 1982; Arakel and McConchie, 1982; Alonso-Zarza, 2003). Therefore, the presence of dolocretes and silcretes in the KSF provide an independent climatic constraint on the depositional environment. Arid to semiarid climate is consistent with other sedimentological evidence such as tepees and the presence of pseudomorphed evaporites (Melezhik and Fallick, in press).

The KSF dolocretes are totally devoid of carbonates with isotopically light carbon (Figs. 4 and 5). This suggests that the carbon isotopic composition of the dolocrete was largely buffered by the substrate dolomite and governed by evaporation. The absence of organic material and photosynthesising bacterial communities in subaerial environments, and the ^{13}C-enriched nature of atmospheric CO_2, were apparently other important factors controlling the carbon isotope composition of the Kuetsjärvi dolocretes.

Isotopic and palaeontological studies of palaeokarsts suggest that subaerial landscapes were intensively occupied by photosynthesising bacteria as far back as 1200 Ma (Beeunas and Knauth, 1985; Horodyski and Knauth, 1994; Kenny and Knauth, 2001). Gutzmer and Beukes (1998) reported possible evidence for terrestrial vegetation dated back 2200–2000 Ma. Geochemical data hint at a possible presence of microbial mats in 2600–2700 Ga soil surface (Watanabe et al., 2000) and 2760 Ma ephemeral ponds (Rye and Holland, 2000). The isotopic data from the 2200 Ma dolocretes formed in the lacustrine rift-bound setting do not suggest that subaerial surface was colonised by microbial mats. Abundant red, iron-stained dolocrete implies that the exposed surfaces were affected by an O_2-rich atmosphere.

5.6. Applications to the Palaeoproterozoic positive excursion of $^{13}C/^{12}C$

The dolocrete formed on and in ^{13}C-rich dolostones which record the 2200 Ma global positive isotopic shift in $^{13}C/^{12}C$ of sedimentary carbonates (Baker and Fallick, 1989a,b; Karhu, 1993), one of the largest in the Earth's history (Melezhik et al., 2000). The KSF dolostones have $\delta^{13}C$ as high as +8‰ (Melezhik and Fallick, 1996) and represent one of the key localities of Palaeoproterozoic ^{13}C-rich carbonate formations. It has been suggested that $\delta^{13}C$ values more than +5‰ may exceed the global $\delta^{13}C$ value for the isotopic shift at ca. 2200 Ma (Melezhik et al., 1997, 1999). If the isotopic excursion were triggered by globally enhanced C_{org} burial (Baker and Fallick, 1989a,b; Karhu, 1993), further enrichment requires an extra ^{13}C-rich source(s) which might not be representative of the coeval global environment. However, the KSF dolostones have been used on several occasions as a key example of the Palaeoproterozoic ^{13}C-rich carbonates (e.g., Karhu, 1993; Melezhik and Fallick, 1996) as well as for construction of the $\delta^{13}C_{carb}$ secular trend in the Palaeoproterozoic (Melezhik et al., 1999). Local factors, which have been considered for enhanced ^{13}C enrichment (Melezhik et al., 1999, 2000), include development of abundant stromatolite-forming microbial communities in shallow-water restricted basins, establishment of evaporative and partly restricted environments combined with high bioproductivity, enhanced uptake of ^{12}C, and penecontemporaneous recycling

of organic material in cyanobacterial mats with the production and consequent loss of CO_2 (and CH_4?).

The presence of numerous subaerial exposure surfaces and dolocretes provide additional constraints on the depositional environments of the KSF ^{13}C-rich dolostones. The exposure surfaces and dolocretes suggest that even if there was connection between the Kuetsjärvi depositional system and the sea, they could have frequently been decoupled. Therefore, the Kuetsjärvi depositional system could hardly have been maintained constantly in isotopic equilibrium with open seawater. Consequently, there was an inevitably significant influence of local factors on the carbon and oxygen isotope composition of the KSF dolostones. Thus, the exposure features and dolocretes impose an additional restriction on use the isotopic composition of the KSF dolostones for reconstruction of the $\delta^{13}C_{carb}$ secular change.

6. Conclusions

1. Limited knowledge of sequence stratigraphy, palaeotectonic, depositional and post-depositional palaeoenvironments of Palaeoproterozoic ^{13}C-rich carbonates hampers the assessment as to whether the measured $\delta^{13}C_{carb}$ values (from +4 to +28‰) reflect global factors or various local factors, or perhaps of a combination of both.
2. The 2200 Ma KSF from the Pechenga Greenstone Belt, NE Fennoscandinavian Shield, represents such a challenging case. The formation is composed of ^{13}C-rich dolostones ($\delta^{13}C = +6.6$ to +7.6‰ V-PDB, $\delta^{18}O = 16.7$ to 21.5‰ V-SMOW) and has been used on several occasions for reconstruction of the Palaeoproterozoic $\delta^{13}C$ secular curve.
3. Numerous subaerial erosion and dissolution surfaces, superficial dolocretes and silcretes, epikarstic phenomena, and surface dissolution cavities covered with hot-water spring travertine crust have been discovered in the ca. 80 m thick ^{13}C-rich dolostone unit of the KSF.
4. The 'vuggy', red, iron-stained, dolomicritic beds capped by silicified nodular crust (dolocrete) show enrichment in ^{18}O, and some resemblance to modern calcretes which formed on the surface by capillary rise and evaporation of dissolved carbonate (per-ascensum calcrete) under arid or semi-arid conditions.
5. Fabrics associated with plant roots and input of terrestrial organic matter, which are all typical for the post-Cretaceous pedogenic calcretes, have not been identified. Alfa fabrics can be applied to describe the dolocrete.
6. Abundant red, iron-stained dolocretes imply the existence of an O_2-rich atmosphere. Isotopic features of the superficial dolocrete do not suggest that the subaerial surface was colonised by microbial mats, and indicate the apparent lack of biological uptake of ^{12}C combined with evaporation during formation of the dolocrete at ca. 2200 Ma ago.
7. A series of superficial dolocrete horizons suggests several episodes of subaerial exposure and frequent decoupling between the Kuetsjärvi depositional system and the bordering sea, and thus high $\delta^{13}C_{carb}$ values reported from the KSF dolostones may not represent the global isotopic signal.

Acknowledgements

This research has been carried out by the Geological Survey of Norway (NGU) jointly with the Scottish Universities Environmental Research Centre (SUERC), Glasgow, Scotland and the University of Cagliari, Italy. Access to core material of the Central Kola and Pechenga Geological Expeditions is acknowledged with thanks. The fieldwork was financially supported by the IGCP Project 408, NGU Project 282200 and INTAS-RFBR 095-928. The isotope analyses were performed at SUERC supported by the Consortium of Scottish Universities and the Natural Environment Research Council. Funds by and access to the EU Geochemical Facilities at the Department of Earth Sciences of the University of Bristol is acknowledged. P. Knauth is warmly acknowledged for providing digital data on C and O isotope composition of dolocretes developed on the basaltic substrate. P. Padget read an earlier version of the manuscript and suggested improvements. B. Fouke, A. Immenhauser, and A. Siedlecka are thanked for constructive comments on the earlier version of the manuscript. J. Karhu and anonymous referee are thanked for timely and constructively critical reviews of the last version of the manuscript.

References

Adams, A.E., 1980. Calcrete profiles in the Eyam Limestone (Carboniferous) of Derbyshire: petrology and regional significance. Sedimentology 27, 550–651.

Allan, J.R., Matthews, R.K., 1982. Isotope signatures associated with early meteoric diagenesis. Sedimentology 29, 797–818.

Alonso-Zarza, A.M., 2003. Palaeoenvironmental significance of palustrine carbonates and calcretes in the geological record. Earth-Sci. Rev. 60, 261–298.

Amelin, Yu.V., Heaman, L.M., Semenov, V.S., 1995. U–Pb geochronology of layered mafic intrusions in the eastern Baltic Shield: implications for the timing and duration of Palaeoproterozoic continental rifting. Precambrian Res. 75, 31–46.

Arakel, A.V., McConchie, D., 1982. Classification and genesis of calcrete and gypsite lithofacies in paleodrainage systems of inland Australia and their relationship to carnotite mineralization. J. Sed. Petrol. 52 (4), 1149–1170.

Ashley, G.M., Renaut, R.W., 2002. Rift sedimentation. In: Renaut, R.W., Ashley, G.M. (Eds.), Sedimentation in Continental Rifts. SEPM Spec. Publ. 73, pp. 3–7.

Baker, A.J., Fallick, A.E., 1989a. Evidence from Lewisian limestones for isotopically heavy carbon in two-thousand-million-year-old sea water. Nature 337, 352–354.

Baker, A.J., Fallick, A.E., 1989b. Heavy carbon in two-billion-year-old marbles from Lofoten-Vesterålen, Norway: Implications for the Precambrian carbon cycle. Geochim. Cosmochim. Acta 53, 1111–1115.

Banner, J.L., Hanson, G.N., 1990. Calculation of simultaneous isotopic and trace-element variations during water-rock interaction with applications to carbonate diagenesis. Geochim. Cosmochim. Acta 54, 3123–3137.

Beeunas, M.A., Knauth, L.P., 1985. Preserved stable isotopic signature of subaerial diagenesis in the 1.2-b.y. Mescal Limestone, central Arizona; implications for the timing and development of a terrestrial plant cover. Geol. Soc. Am. Bull. 96, 737–745.

Behr, 2002 Behr, H.-J., 2002. Magadiite and Magadi chert: a critical analysis of the silica sediments in the lake Magadi basin, Kenya. In: Renaut, R.W., Asley, G.M. (Eds.), Sedimentation in Continental Rifts. Soc. Econ. Paleontol. Mineral. Spec. Publ. 73, pp. 257–273.

Bekker, A., Kaufman, A.J., Karhu, J.A., Beukes, N.J., Swart, Q.D., Coetzee, L.L., Eriksson, K.A., 2001. Chemostratigraphy of the Paleoproterozoic Duitschland Formation, South Africa; implications for coupled climate change and carbon cycling. Am. J. Sci. 301, 261–285.

Bekker, A., Karhu, J.A., Eriksson, K.A., Kaufman, A.J., 2003. Chemostratigraphy of Palaeoproterozoic carbonate successions of the Wyoming Craton: tectonic forcing of biogeochemical change? Precambrian Res. 120, 279–325.

Bertrand-Sarfati, J., Moussine-Pouchkine, A., 1983. Pedogenetic and diagenetic fabrics in the Upper Proterozoic Sarnyéré Formation (Gourma Mali). Precambrian Res. 20, 225–242.

Blank, H.R., Tynes, E.W., 1965. Formation of caliche in situ. Geol. Soc. Am. Bull. 76, 1387–1391.

Blatt, H., Middleton, G., Murray, R., 1980. Origin of Sedimentary Rocks. Prentice-Hall, Englewood Cliffs.

Bretz, J.H., Horberg, L., 1949. Caliche in southeastern New Mexico. J. Geol. 57, 491–511.

Brewer, R., 1964. Fabric and Mineral Analysis of Soil. Wiley, New York, 470 pp.

Buick, I.S., Uken, R., Gibson, R.L., Wallmach, T., 1998. High-$\delta^{13}C$ Paleoproterozoic carbonates from the Transvaal Supergroup, South Africa. Geology 26, 875–878.

Carlisle, D., 1983. Concentration of uranium and vanadium in calcrets and gypsites. In: Wilson, R.C.L. (Ed.), Residual Deposits. Geol. Soc. Lond. Spec. Publ. 11, 185–195.

Cander, H., 1995. Interplay of water–rock interaction efficiency, unconformities, and fluid flow in a carbonate aquifer; Floridan Aquifer system. In: Budd, D.A., Saller, A.H., Harris, P.M. (Eds.), Unconformities and Porosity in Carbonate Strata. AAPG Mem. 63, 103–124.

Cerling, T.E., Quade, J., Wang, Y., Bowman, J.R., 1989. Carbon isotopes in soils and paleosols as ecology and paleoecology indicators. Nature 341, 138–139.

Chafetz, H.S., Lawrence, J.R., 1994. Stable isotopic variability within modern travertines. Geographie physique et Quaternaire 48, 257–273.

Chown, E.H., Caty, J.-L., 1983. Diagenesis of the Aphebian Mistassini regolith, Quebec, Canada. Precambrian Res. 19, 285–299.

Demicco, R.V., Hardie, L.A., 1994. Sedimentary structure and early diagenetic features of shallow marine carbonate deposits. SEPM Atlas Series, No. 1. Tulsa, OK, USA, 265 pp.

Dickson, J.A.D., Saller, A.H., 1995. Identification of subaerial exposure surfaces and porosity preservation in Pennsylvanian and Lower Permian shelf limestones, eastern Central Basin Platform, Texas. In: Budd, D.A., Saller, A.H., Harris, P.M. (Eds.), Unconformities and Porosity in Carbonate Strata. AAPG Mem. 63, 239–257.

Driese, S.G., Mora, C.I., 2002. Paleopedology and stable-isotope geochemistry of Late Triassic (Carnian-Norian) paleosols, Durham sub-basin, North Caroline, USA: implications for paleoclimate and paleoatmospheric pCO_2. In: Renaut, R.W., Ashley, G.M. (Eds.), Sedimentation in Continental Rifts. SEPM Spec. Publ. 73, pp. 205–218.

Esteban, M., Klappa, C.F., 1983. Subaerial exposure environment. In: Scholle, P.A., Bebout, D.G., Moore, C.H. (Eds.), Carbonate Depositional Environments. Am. Assoc. Petrol. Geol. Mem. 33, 1–54.

Fairchild, I., Marshall, J.D., Bertrand-Sarafati, J., 1990. Stratigraphic shifts in carbon isotopes from Proterozoic stromatolitic carbonates (Mauritania): influence of primary mineralogy and diagenesis. Am. J. Sci. 290A, 46–79.

Fantidis, J., Ehhalt, D.H., 1970. Variations of carbon and oxygen isotope composition in stalagmites and stalactites—evidence of nonequilibrium isotopic fractionation. Earth Planet. Sci. Lett. 10, 136–144.

Fornaca-Rinaldi, G., Panichi, C., Tongiorgio, E., 1968. Some causes of the variation of the isotopic composition of carbon and oxygen in cave concretions. Earth Planet. Sci. Lett. 4, 321–324.

Fouke, B.W., Farmer, J.D., Des Marais, D.J., Pratt, L., Sturchio, N.C., Burns, P.C., Discipulo, M.K., 2000. Depositional facies and aqueous-solid geochemistry of travertine-depositing hot springs (Angel Terrace, Mammoth Hot Springs, Yellowstone National Park, USA). J. Sed. Res. 70, 565–585.

Freytet, P., 1973. Petrography and paleo-environment of continental carbonate deposits with particular reference to the Upper Cretaceous and Lower Eocene of Languedoc (southern France). Sed. Geol. 10, 25–60.

Freytet, P., Plazait, J.C., 1982. Continental carbonate sedimentation and pedogenesis—Late Cretaceous and Early Tertiary of south France. In: Puser, B.H. (Ed.), Contrib. Sed. 12. Schweizertische Verlagsbuchhandling, Stutgart, 213 pp.

Friedman, I., 1970. Some investigations of deposition of travertine from hot springs. I. The isotopic chemistry of a travertine-depositing spring. Geochim. Cosmochim. Acta 34, 1303–1315.

Goldstein, R.H., Anderson, J.E., Bowman, M.W., 1991. Diagenetic responses to sea-level change; integration of field, stable isotope, paleosol, paleokarst, fluid inclusion, and cement stratigraphy research to determine history and magnitude of sea-level fluctuation. In: Franseen, E.K., Watney, W.L., St. Kendall, C.G.-C., Ross, W. (Eds.), Sedimentary Modeling: Computer Simulations and Methods for Improved Parameter Definition. Kansas, State Geol. Surv. Bull. 233, 139–162.

Gonfiantini, R., Panichi, C., Tongiorgi, E., 1968. Isotopic disequilibrium in travertine deposition. Earth Planet. Sci. Lett. 5, 55–58.

Goudie, A., 1973. Duricrusts in Tropical and Subtropical Landscapes. Clarendon Press, Oxford, 174 pp.

Goudie, A., 1983. Calcrete. In: Goudie, A.S., Kenneth, P. (Eds.), Chemical Sediments and Geomorphology: Precipitates and Residua in the Near-Surface Environment. Academic Press, London, pp. 93–131.

Guo, L., Andrews, J., Riding, R., Dennis, P., Dresser, Q., 1996. Possible microbial effects of stable carbon isotopes in hot-spring travertines. J. Sed. Res. 66, 468–473.

Gutzmer, J., Beukes, N.J., 1998. Earliest laterites and possible evidence for terrestrial vegetation in the Early Proterozoic. Geology 26, 263–266.

Hanski, E.J., Huhma, H., Smolkin, V.F., Vaasjoki, M., 1990. The age of ferrropicritic volcanism and comagmatic Ni-bearing intrusions at Pechenga, Kola Peninsula, USSR. Geol. Soc. Finland Bull. 62, 123–133.

Harrison, R.S., Steinen, R.O., 1978. Subaerial crusts, caliche profiles, and breccia horizons: comparison of some Holocene and Mississippian exposure surfaces, Barbados and Kentucky. Geol. Soc. Am. Bull 89, 385–396.

Hay, R.L., Leeder, R.J., 1978. Calcretes of Olduvai Gorge and the Ndolanya Beds of northern Tanzania. Sedimentology 25, 649–673.

Hendy, C.H., 1971. The isotopic geochemistry of speleothems. I. The calculation of the effect of different modes of formation on the isotopic composition of speleothems and their applicability as paleoclimatic indicators. Geochim. Cosmochim. Acta 35, 801–824.

Horodyski, R.J., Knauth, L.P., 1994. Life on land in the Precambrian. Science 263, 494–498.

Hsu, K.J., Siegenthaller, C., 1969. Preliminary experiments on hydrodynamic movement induced by evaporation and their bearing on the dolomite problem. Sedimentology 12, 11–25.

Jacobsen, S.B., Kaufman, A.J., 1999. The Sr, C and O isotopic evolution of Neoproterozoic seawater. Chem. Geol. 161, 37–57.

James, N.P., 1972. Holocene and Pleistocene calcareous crust (caliche) profiles: criteria for subaerial exposure. J. Sed. Petrol. 42, 817–836.

James, N.P., 1984. Shallowing-upwards sequences in carbonates. In: Walker, R.G. (Ed.), Facies Model, second ed. Geoscience Canada Reprint Series 1, St. Johns, Newfoundland, pp. 213–228.

Johnson, D.B., Swett, K., 1974. Origin and diagenesis of calcitic and haematitic nodules in the Jordan sandstones of NE Iowa. J. Sed. Petrol. 44, 790–794.

Jones, B., Renaut, R.W., Rosen, M.R., 1996. High-temperature (>90°C) calcite precipitation at Waikite Hot Springs, North Island, New Zealand. J. Geol. Soc. Lond. 153, 481–496.

Kahle, C.F., 1997. Origin of subaerial Holocene calcareous crusts—role of algae, fungi, and sparmicritization. Sedimentology 24, 413–435.

Karhu, J.A., 1993. Palaeoproterozoic evolution of the carbon isotope ratios of sedimentary carbonates in the Fennoscandian Shield. Geol. Surv. Finland Bull. 371, 1–87.

Karhu, J.A., Melezhik, V.A., 1992. Carbon isotope systematics of early Proterozoic sedimentary carbonates in the Kola Peninsula, Russia: correlations with Jatulian formations in Karelia. In: Balagansky, V.V., Mitrofanov, F.P. (Eds.), Correlations of Precambrian Formations of the Kola-Karelia Region and Finland. Kola Scientific Centre of the Russian Academy of Sciences, Apatity, pp. 48–53.

Kenny, R., Knauth, L.P., 2001. Stable isotope variations in the Neoproterozoic Beck Spring Dolomite and Mesoproterozoic Mescal Limestone paleokarst; implications for life on land in the Precambrian. Geol. Soc. Am. Bull. 113, 650–658.

Klappa, C.F., 1980. Brecciation texture and tepee structures in Quaternary calcrete (caliche) profiles from eastern Spain—the plant factor in their formation. J. Geol. 15, 81–89.

Klimchouk, A., 1997. The nature and principal characteristics of epikarst. In: Yves, J.P. (Ed.), Proceedings of the 12th International Congress of Speleology: Symposium 7, Physical Speleology; Symposium 8: Karst Geomorphology, vol. 12, p. 306.

Knauth, L.P., Brilli, M., Klonowski, S., 2003. Isotope geochemistry of caliche developed on basalt. Geochim. Cosmochim. Acta 67, 185–195.

Mann, A.W., Horwitz, R.C., 1979. Groundwater calcrete deposits in Australia: some observations from western Australia. J. Geol. Soc. Aust. 26, 293–303.

Manze, U., Brunnacker, K., 1977. Ûber das verhalten der Sauerstuff- und Kohlenstoff-isotope in Kalkkrusten and kalktuffen des Mediterranean Raunes und der Sahara. Zeitschrift für Geomorphologie 21, 345–353.

Mazzullo, S.J., Birdwell, B.A., 1989. Syngenetic formation of grainstones and pisolites from fenestral carbonates in peritidal settings. J. Sed. Petrol. 59, 605–611.

McCrea, J.M., 1950. On the isotopic chemistry of carbonates and a paleotemperature scale. J. Chem. Phys. 18, 849–857.

Melezhik, V.A., Fallick, A.E., 1996. A widespread positive $\delta^{13}C_{carb}$ anomaly at around 2.33–2.06 Ga on the Fennoscandian Shield: a paradox? Terra Nova 8, 141–157.

Melezhik, V.A., Fallick, A.E., 2001. Palaeoproterozoic ^{13}C-rich travertines from a rift lake environment. Chem. Geol. 173, 293–312.

Melezhik, V.A., Fallick, A.E., 2003. $\delta^{13}C$ and $\delta^{18}O$ variations in primary and secondary carbonate phases: several contrasting examples from Palaeoproterozoic ^{13}C-rich metamorphosed dolostones. Chem. Geol. 201, 213–228.

Melezhik, V.A., Fallick, A.E., in press. The Palaeoproterozoic, rift-related, ^{13}C-rich, lacustrine carbonates, NW Russia. Part I. Sedimentology and major element geochemistry. Trans. R. Soc. Edin.: Earth Sci.

Melezhik, V.A., Sturt, B.A., 1994. General geology and evolutionary history of the early Proterozoic Polmak-Pasvik-Pechenga-Imandra/Varzuga-Ust'Ponoy Greenstone Belt in the north-eastern Baltic Shield. Earth-Sci. Rev. 36, 205–241.

Melezhik, V.A., Fallick, A.E., Clark, T., 1997. Two billion year old isotopically heavy carbon: evidence from the Labrador Trough, Canada. Can. J. Earth Sci. 34, 271–287.

Melezhik, V.A., Fallick, A.E., Medvedev, P.V., Makarikhin, V.V., 1999. Extreme $^{13}C_{carb}$ enrichment in ca. 2.0 Ga magnesite–stromatolite–dolomite–'red beds' association in a global context: a case for the world-wide signal enhanced by a local environment. Earth-Sci. Rev. 48, 71–120.

Melezhik, V.A., Fallick, A.E., Medvedev, P.V., Makarikhin, V.V., 2000. Palaeoproterozoic magnesite–stromatolite–dolostone–'red bed' association, Russian karelia: palaeoenvironmental constraints on the 2.0 Ga positive carbon isotope shift. Norsk geol. Tidsskrift 80, 163–186.

Melezhik, V.A., Fallick, A.E., Smirnov, Yu.P., Yakovlev, Yu.N., 2003. Fractionation of carbon and oxygen isotopes in ^{13}C-rich Palaeoproterozoic dolostones in the transition from medium-grade to high-grade greenschist facies: a case study from the Kola Superdeep Drillhole. J. Geol. Soc. Lond. 160, 71–82.

Meyers, W.J., 1977. Chertification in the Mississippian Lake Valley Formation, Sacramento Mountains, New Mexico. Sedimentology 24, 75–105.

Multer, H.G., Hoffmeister, J.E., 1968. Subaerial laminated crusts of the Florida Keys. Geol. Soc. Am. Bull. 79, 183–192.

Mutti, M., 1995. Porosity development and diagenesis in the Orfento Supersequence and its bounding unconformities (Upper Cretaceous, Montagna della Maiella, Italy). In: Budd, D.A., Saller, A.H., Harris, P.M. (Eds.), Unconformities and Porosity in Carbonate Strata. AAPG Mem. 63, 141–158.

Read, J.F., 1976. Calcretes and their distinction from stromatolites. In: Walter, M.R. (Ed.), Stromatolites. Elsevier, Amsterdam, pp. 55–71.

Reeves Jr., C.C., 1970. Origin, classification and geological history of caliche on the southern High Plains, Texas and eastern New Mexico. J. Geol. 78, 352–362.

Reeves Jr., C.C., 1976. Caliche; Origin, Classification, Morphology and Uses. Estacado Books, Lubbock, TZ, 233 pp.

Robbin, D.M., Stipp, J.J., 1974. Depositional rate of laminated soilstone crusts, Florida Keys. J. Sed. Petrol. 49, 175–180.

Rosenbaum, J.M., Sheppard, S.M.F., 1986. An isotopic study of siderites, dolomites and ankerites at high temperatures. Geochim. Cosmochim. Acta 50, 1147–1159.

Rye, R., Holland, H.D., 2000. Life associated with a 2.76 Ga ephemeral pond? Evidence from Mount Roe #2 paleosol. Geology 28, 483–486.

Salomons, W., Goudie, A., Mook, W.G., 1978. Isotopic composition of calcrete deposits from Europe, Africa and India. Earth Surf. Proc. 3, 43–57.

Schidlowski, M., Eichmann, R., Junge, C.E., 1976. Carbon isotope geochemistry of the Precambrian Lomagundi carbonate province, Rhodesia. Geochim. Cosmochim. Acta 40, 449–455.

Shinn, E.A., 1983. Tidal flat environment. In: Scholle, P.A., Bebout, D.G., Moore, C.H. (Eds.), Carbonate Depositional Environments AAPG Mem. 33, 173–210.

Shinn, E.A., 1986. Modern carbonate tidal flats: their diagnostic features. Quaternary J. Colorado School of Mines 81, 7–35.

Smale, D., 1973. Silcretes and associated silica diagenesis in southern Africa and Australia. J. Sed. Petrol. 43, 1077–1089.

Sochava, A.V., Savel'e, A.A., Schuleshko, J.K., 1975. Caliche in the Middle Proterozoic sequence of central Karelia. Trans. Russ. Acad. Sci. 233, 173–176.

Summerfield, M.A., 1982. Distribution, nature and probable genesis of silcrete in arid and semi-arid southern Africa. In: Yaalon, D.H. (Ed.), Aridic Soils and Geomorphic Processes. Catena Supplement 1, Braunschweig, pp. 37–65.

Summerfield, M.A., 1983. Silcrete. In: Goudie, A.S., Kenneth, P. (Eds.), Chemical Sediments and Geomorphology: Precipitates and Residua in the Near-Surface Environment. Academic Press, London, pp. 59–90.

Tucker, M.E., 1982. Precambrian dolomites: petrographic and isotopic evidence that they differ from Phanerozoic dolomites. Geology 10, 7–12.

Wagner, D., Tasker, D.R., Wahlman, G.P., 1995. Reservoir degradation and compartmentalization below subaerial unconformities; limestone examples from West Texas, China, and Oman. In: Budd, D.A., Saller, A.H. and Harris, P.M. (Eds.), Unconformities and Porosity in Carbonate Strata. AAPG Mem. 63, 177–194.

Walls, R.A., Harris, W.B., Nuna, W.E., 1975. Calcareous crust (caliche) profiles and early subaerial exposures of Carboniferous carbonates, northeastern Kentucky. Sedimentology 22, 417–440.

Watanabe, Y., Martini, J.E., Ohmoto, H., 2000. Geochemical evidence for terrestrial ecosystems 2.6 billion years ago. Nature 408, 574–578.

Wolfbauer, C.A., Surdam, R.C., 1974. Origin of non-marine dolomite in Eocene Lake Gosiute, Green River Basin, Wyoming. Geol. Soc. Am. Bull. 85, 1733–1740.

Woodrow, D.L., Fletcher, F.W., Abrnsbrak, W.F., 1973. Paleogeography and paleoclimate at the deposition site of the Devonian Catskill and Old Red Facies. Geol. Soc. Am. Bull. 85, 3051–3064.

Wright, V.P., 1989. Terrestrial stromatolites and laminar calcretes—a review. Sed. Geol. 65, 1–13.
Wright, V.P., 1990. Syngenetic formation of grainstones and pisolites from fenestral carbonates in peritidal settings—discussion. J. Sed. Petrol. 60, 309–310.
Wright, V.P., Tucker, M.E., 1991. Calcrete, an introduction. In: Wright, V.P., Tucker, M.E. (Eds.), Assoc. Sed. Rep. Ser. 2, 1–22.
Yudovich, Ya.E., Makarikhin, V.V., Medvedev, P.V., Sukhanov, N.V., 1991. Carbon isotope anomalies in carbonates of the Karelian Complex. Geochem. Int. 28, 56–62.